Diffraction in high-energy onium - nucleus scattering and structure of partonic evolution

Internship Report

By

Dung LE ANH

Program: Master 2 in High Energy Physics

Under the supervision of:

M. Stéphane Munier

ÉCOLE POLYTECHNIQUE, UNIVERSITÉ PARIS - SACLAY
September 2018

ÉCOLE POLYTECHNIQUE, UNIVERSITÉ PARIS - SACLAY

Abstract

Master 2 in High Energy Physics

Diffraction in high-energy onium - nucleus scattering

and structure of partonic evolution

by Dung LE ANH

A fast-moving hadron, due to quantum fluctuations, is a set of many soft gluons. The wave function of a small hadron can be obtained as the solution of an evolution equation, which is most conveniently formulated in the so-called color dipole model. This model also enables us to describe the diffractive onium-nucleus scattering in which there is a range of rapidity around the nucleus with no particles observed. In this report, the diffraction in the high-energy onium - nucleus scattering will be presented and related to the genealogy of the partonic evolution which appears as a dipole branching-diffusion process. This relation will then be tested numerically. In addition, an analogy to the genealogy of the one dimensional branching random walks will be mentioned. Further considerations and outlook will be also discussed.

Acknowledgements

First of all, I would like to express my sincere gratitude to my advisor M. **Stéphane Munier** for the continuous and thorough support during my internship, for his patience, motivation, and immense knowledge. The door to his office was always open whenever I ran into a trouble spot or had questions related to not only the project but also other aspects of the academic training.

Beside my advisor, I am also grateful to **Giuliano Giacalone** (PhD student at IPhT, CEA Saclay) and M. **Cédric Lorce** (CPhT, École Polytechnique) for extremely useful discussions and helps during my work.

I also take this opportunity to express gratitude to all members of the particle physics group in CPhT, École Polytechnique for their kindness and helps in whole time I worked at CPhT as an internship student.

Last but not the least, I would like to thank my family and my friends for supporting me spiritually throughout every aspect of my life.

Contents

Preface

The field of high energy QCD has been developing rapidly over the past few decades, generating vast amount of interesting results in both theoretical and experimental aspects. At high energies, or small values of the longitudinal momentum fraction x, it is possible to observe more quantum fluctuations of incoming objects, hence the QCD dynamics in this regime becomes sophisticated.

In the evaluation of Feynman diagrams in the small-x regime, the coupling constant α_s always comes with "infrared" logarithm, namely $\ln(1/x)$. Perturbative series in $\alpha_s \ln(1/x)$ is necessary to be fully resummed, which is performed by the Balitsky-Fadin-Kuraev-Lipatov (BFKL) [1–3] evolution equation. This linear equation, however, seems to violate the unitarity at ultrahigh energy. Therefore, nonlinear correction is required, which is taken into account, for example, in the Balitsky - Kovchegov (BK) equation [4, 5]. The derivations of these equations could be based on Mueller's color dipole model [6–8], which is a very elegant way to represent QCD in high energy limit.

The color dipole model could be then used to describe the diffractive onium-nucleus scattering for which there is a region in rapidity around the nucleus with no particles seen. In fact, the onium-nucleus scattering could be studied experimentally from the electron-nucleus scattering for the following reason: the photon, which mediates the electron-nucleus interaction, can be resolved as a pair of quark and anti-quark (onium) during the interaction in some boosted frames. Studies of diffraction at very high energy turn out to be interesting for the theoretical understanding of QCD, and relevant for phenomenology at a future electron-ion collider.

The layout of the report is as follows. Chapter 1 presents an overview of pertubative QCD and small-x physics. The light-cone formalism, which will be employed throughout the report, is also introduced. Chapter 2 gives a review of the color dipole model and discussions on the BK and BFKL evolution equations in this framework. Chapter 3 is dedicated to present the main results of the report. In this chapter, we will discuss the diffractive onium - nucleus scattering and its relation to ancestry in the partonic evolution. Finally, a summary and further developments are given in the Conclusion.

Chapter 1

An overview of perturbative QCD and small-x physics

Quantum chromodynamics (QCD) is the quantum field theory of strong interaction. Due to the behavior of (running) coupling α_s, which is small at short distances and becomes larger at longer distances, the study of QCD could be divided into perturbative and non-perturbative regimes. This chapter is dedicated for reviewing perturbative QCD on the light-cone and some aspects of QCD at small Bjorken - x.

1.1 QCD as a non-abelian gauge theory

QCD is a gauge field theory whose gauge group is non-abelian SU(3) describing the strong interaction sector of the Standard Model. It deals with quarks (anti-quarks) and gluons, which do not exist as free but combine to form hadronic bound states. Quarks, denoted by $q_i(x)$, are spin-$\frac{1}{2}$ Dirac fields of color i ($i = 1, 2, 3$) in the fundamental representation **3** (triplet) of the color SU(3), while anti-quarks, $\bar{q}_i(x)$, are in the complex conjugate representation $\bar{\mathbf{3}}$. On the other hand, gluons are described by the spin-1 field $A^a_\mu(x)$ of zero mass and color index a ($a = \overline{1, 8}$) in the adjoint representation (color octet) of the SU(3) gauge group. The strong interactions among quarks and gluons are formulated in following Lagrangian [9–11]:

$$\mathfrak{L}_{QCD} = \sum_{\text{flavors}} \bar{q}_i (i\gamma^\mu D_\mu - m)_{ij} q_j - \frac{1}{4} G^{\mu\nu}_a G^a_{\mu\nu} \tag{1.1}$$

where the covariant derivative is defined as:

$$D_\mu = \partial_\mu - i g_s t^a A^a_\mu \tag{1.2}$$

The strong coupling g_s is the QCD analogy of the electromagnetic coupling e in QED, and t^a are generators of SU(3) in the fundamental representation encoding the color structure of gluons and interactions among quark and gluon degrees of freedom. These color matrices are usually chosen to be the Gell-Mann matrices λ^a, $t^a = \frac{\lambda^a}{2}$, and satisfy the following commutation relation:

$$[t^a, t^b] = i f^{abc} t^c \tag{1.3}$$

where f^{abc} are the structure constants of SU(3). The antisymmetric non-abelian field tensor $G^a_{\mu\nu}$ in eq.(1.1) is defined as:

$$G^a_{\mu\nu} = \partial_\mu A^a_\nu - \partial_\nu A^a_\mu + g_s f^{abc} A^b_\mu A^c_\nu \tag{1.4}$$

Unlike photons in QED, gluons themselves carry color charge, which leads to the self-interaction of gluons encoded in the term $(g_s f^{abc} A^b_\mu A^c_\nu)$ in the field tensor (1.4). The gluon self-interaction, when performing the perturbative calculations, gives rise to the vacuum polarization diagrams with gluon loops, which result in the different behavior of the running coupling with respect to the QED running coupling.
As QCD is a gauge theory, it has the gauge symmetry, which means that the Lagrangian (1.1) is invariant under the following local SU(3) transformation:

$$\begin{aligned} q(x) &\rightarrow U(x)q(x), \qquad \bar{q}(x) \rightarrow \bar{q}(x)U^{-1}(x) \\ A_\mu(x) &\rightarrow U(x)A_\mu(x)U^{-1}(x) - \tfrac{i}{g_s}\left[\partial_\mu U(x)\right]U^{-1}(x) \end{aligned} \tag{1.5}$$

where $A_\mu = t^a A^a_\mu$ and the transformation matrix $U(x)$ is given by:

$$U(x) = \exp\left(it^a\theta^a(x)\right) \tag{1.6}$$

with $\theta^a(x)$ is an arbitrary set of real functions of space-time coordinates. Under this gauge transformation, the covariant derivative and the field strength tensor are transformed as:

$$D_\mu \rightarrow U(x)D_\mu U^{-1}(x), \quad G^a_{\mu\nu} \rightarrow U(x)G^a_{\mu\nu}U^{-1}(x) \tag{1.7}$$

One importance of the gauge symmetry is that physical observables are independent of the choice of gauge in which the calculation is implemented. This fact allows us to choose the most convenient gauge for the practical purpose. However, the gauge invariance introduces the gauge redundancy, i.e, the redundant components in vector potential due to the gauge transformation. Such redundancy could be handled using gauge fixing which will be mentioned in the upcoming section.

1.2 Light-cone perturbation theory

Despite the fact that covariant Feynman quantization (see, for e.g, [12, 13]) based on the instant coordinates is widely used in constructing the field theory, it gives complexity when going beyond the one-loop calculation. In 1949, Dirac [14] pointed out that the instant time t is not the only possible evolution variable. In fact, one can define another evolution parameter which is called the light-cone time x^+ (as defined below) in which 7 out of 10 generators of the Poincaré group are kinematic. Various elegant advantages of the light-cone parameterization which were shown in different works (see, for e.g, [15–19]) make it attractive to be used to describe relativistic systems, especially high energy scattering.
For every four-vector u^μ, the light-cone variables are defined as follows:

$$u^\pm = u^0 \pm u^3, \quad u_\perp = (u^1, u^2) \tag{1.8}$$

and u^μ will be represented as $(u^+, u^-, u_\perp)$. In this light-cone notation, the scalar product becomes:

$$u \cdot v = \frac{1}{2}u^+v^- + \frac{1}{2}u^-v^+ - u_\perp v_\perp \tag{1.9}$$

and, hence, non-zero components of the metric are:

$$g_{+-} = g_{-+} = \frac{1}{2}, \quad g_{11} = g_{22} = -1 \tag{1.10}$$

We see that, for a particle moving with speed of light in $(+z)$ direction, the light-cone coordinate $x^- = 0$ and x^+ increases along the particle's trajectory. Therefore, x^+ is usually interpreted as the light-cone time. Consequently, the "minus" momentum operator P^-, which generates translations in x^+, is understood as the light-cone Hamiltonian.
The choice of the light-cone time variable x^+ is equivalent to the foliation of space-time into space-like hypersurfaces $x^+ = \text{const}$. There are seven Poincaré generators leaving these hypersurfaces invariant

including the momentum operators $(P_\perp, P^+)$. They are called kinematic operators. Since kinematic operators which commute with the Hamiltonian can be used to characterize the quantum states of particles, the states can be specified as $|p^+, x_\perp, \lambda\rangle$ in the light-cone framework, where λ denotes the polarization. Consequently, it is possible to limit our investigation in the transverse plane. One can also notices that the on-shell condition $p^2 = m^2$ results in:

$$p^- = \frac{m^2 + p_\perp^2}{p^+} \tag{1.11}$$

which is simpler than the expression $p^0 = \sqrt{\boldsymbol{p}^2 + m^2}$ in the instant form, which in part makes calculations in the standard Feynman perturbation theory become complicated.

With the light-cone formalism, one can construct the light-cone perturbation theory (LCPT). As mentioned above, there is a gauge redundancy since QCD is a gauge theory. To deal with this fact, we will work in the following gauge:

$$A^+ = 0 \tag{1.12}$$

This is called the light-cone gauge, which can be obtained from the light-cone gauge definition $\eta \cdot A = 0$ with $\eta^\mu = (0, 1, 0_\perp)$ (null vector). We now decompose the quark fields $q(x)$ into $q(x) = q_+(x) + q_-(x)$ with $q_\pm(x) = \frac{1}{2}\gamma^0\gamma^\pm q(x)$ and use the two-component form:

$$\begin{aligned} q &= (\varphi \quad \chi)^T, \quad q_+ = (\varphi \quad 0)^T, \quad q_- = (0 \quad \chi)^T \\ \chi &= \frac{1}{i\partial^+}\left(\hat{\sigma}^i(i\partial^i + g_s A^i) + im\right)\varphi \end{aligned} \tag{1.13}$$

here we use the fact that q_- is not an independent degree of freedom but can be expressed in term of q_+ (via the equation of motion). In this two-component form with the light-cone gauge, interaction Hamiltonian density reads []:

$$\begin{aligned} \mathcal{H}_{int} =& g_s\varphi^\dagger\left[-2\frac{1}{\partial^+}(\partial_\perp \cdot A_\perp) + (\hat{\sigma}_\perp \cdot A_\perp)\frac{1}{\partial^+}(\hat{\sigma}_\perp \cdot \partial_\perp + m) + \frac{1}{\partial^+}(\hat{\sigma}_\perp \cdot \partial_\perp - m)\hat{\sigma}_\perp \cdot A_\perp\right]\varphi \\ &+ g_s f^{abc}\left[\partial^i A_a^j A_b^i A_c^j + \partial^i A_a^i \frac{1}{\partial^+}(A_b^j \partial^+ A_c^j)\right] + \frac{g_s^2}{4} f^{abc} f^{ade} A_b^i A_c^j A_d^i A_e^j \\ &+ g_s^2 \varphi^\dagger(\hat{\sigma}_\perp \cdot A_\perp)\frac{1}{i\partial^+}(\hat{\sigma}_\perp \cdot A_\perp)\varphi + 2g_s^2 \frac{1}{\partial^+}(f^{abc} A_b^j \partial^+ A_c^j)\frac{1}{\partial^+}(\varphi^\dagger t^a \varphi) \\ &+ 2g_s^2 \frac{1}{\partial^+}(\varphi^\dagger t^a \varphi)\frac{1}{\partial^+}(\varphi^\dagger t^a \varphi) + \frac{g_s^2}{2} f^{abc} f^{ade}\frac{1}{\partial^+}(A_b^j \partial^+ A_c^j)\frac{1}{\partial^+}(A_b^j \partial^+ A_c^j) \end{aligned} \tag{1.14}$$

where $\hat{\sigma}^1 = \sigma^2$, $\hat{\sigma}^2 = -\sigma^1$ (σ^i are Pauli matrices) and $(1/\partial^+)$ is defined as:

$$\frac{1}{\partial^+} f(x) = \frac{1}{4}\int dy\, [\theta(x-y) - \theta(y-x)]\, f(y) \tag{1.15}$$

In the Hamiltonian (1.14), the first three terms in the first two lines correspond to quark-gluon, three-gluon and four-gluon vertices, respectively. The remaining terms describe new four-quanta interactions with instantaneous quark and gluon propagators. The rules for the QCD LCPT are listed in the Appendix A. We will now begin the discussion about some aspects of the small-x physics with the cornerstones of pertubative QCD: the parton model of deep inelastic scattering (DIS) and the DGLAP evolution.

1.3 DGLAP evolution

One of the scattering processes of interest in the QCD is the deep inelastic electron-proton scattering where the $e - p$ interaction is mediated by a virtual photon as illustrated in Fig. 1.1.

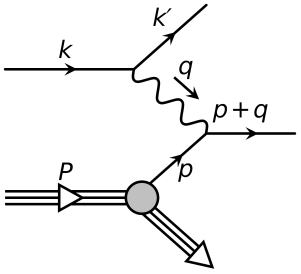

FIGURE 1.1: Diagrammatic illustration of the DIS.

Related variables are defined as:

$$q = k - k', \quad Q^2 = -q^2, \quad x = \frac{Q^2}{2P \cdot q}, \quad W^2 = (P+q)^2 \tag{1.16}$$

The Bjorken-x variable could be interpreted as the fraction of the proton's light-cone momentum carried by the parton struck by the photon, $x = \frac{p^+}{P^+}$. Since $\frac{1}{x} \approx \frac{W^2}{Q^2}$ with $W^2 \gg Q^2$, small x values correspond to high center-of-mass energies. The DIS cross section can be written as [13]:

$$\frac{d\sigma^{ep}}{dE'd\Omega} = \frac{\alpha_{em}^2}{4E^2 \sin^4 \frac{\theta}{2}} \left[W_2(x, Q^2) \cos^2 \frac{\theta}{2} + 2W_1(x, Q^2) \sin^2 \frac{\theta}{2} \right] \tag{1.17}$$

where E and E' are energies of incoming and outgoing electrons, respectively, and W_1 and W_2 are scalar structure functions which have the dimension of inverse mass. It is more convenient to use dimensionless structure functions F_1 and F_2 defined as:

$$F_1(x, Q^2) = mW_1(x, Q^2), \qquad F_2(x, Q^2) = \frac{Q^2}{2mx} W_2(x, Q^2) \tag{1.18}$$

In the naive parton model, we have the following relation [20]:

$$F_2 = 2xF_1 = \sum_f e_f^2 x q^f(x) \tag{1.19}$$

where $q^f(x)$ is the quark distribution function, which is the probability of finding a quark of type f (with charge e_f) with momentum fraction x inside the proton. The Q-independent behavior of the functions F_1 and F_2 is known as Bjorken scaling [21] and characterizes for the DIS on a point-like particle.

The ep interaction is, however, more complicated than in the naive parton model due to QCD corrections. One increases the virtuality Q^2, the proton is probed with higher resolution. Consequently, the parton distribution functions now depend on the momentum scale Q^2.

Parton distribution functions are non-perturbative objects, but their variation in term of the virtuality Q^2 can be described perturbatively. The Q^2 evolution of the parton distribution functions is formulated in the so-called DGLAP equations [22–24]:

$$\frac{\partial \Delta^{f\bar{f}}(x, Q^2)}{\partial \ln Q^2} = \frac{\alpha_s(Q^2)}{2\pi} \int_x^1 \frac{dz}{z} P_{qq}(z) \Delta^{f\bar{f}}(\frac{x}{z}, Q^2) \tag{1.20}$$

$$\frac{\partial}{\partial \ln Q^2} \begin{pmatrix} \Sigma(x, Q^2) \\ G(x, Q^2) \end{pmatrix} = \frac{\alpha_s(Q^2)}{2\pi} \int_x^1 \frac{dz}{z} \begin{pmatrix} P_{qq}(z) & P_{qg}(z) \\ P_{gq}(z) & P_{gg}(z) \end{pmatrix} \begin{pmatrix} \Sigma(x/z, Q^2) \\ G(x/z, Q^2) \end{pmatrix} \tag{1.21}$$

where $\Delta^{f\bar{f}}(x,Q^2)$ and $\Sigma(x,Q^2)$ are the flavor non-singlet distribution function and the flavor singlet distribution function, respectively:

$$\Delta^{f\bar{f}}(x,Q^2) = q^f(x,Q^2) - q^{\bar{f}}(x,Q^2) \tag{1.22}$$

$$\Sigma(x,Q^2) = \sum_f \left[q^f(x,Q^2) + q^{\bar{f}}(x,Q^2)\right] \tag{1.23}$$

and $G(x,Q^2)$ and $q^f(x,Q^2)$ ($q^{\bar{f}}(x,Q^2)$) are, correspondingly, the gluon and quark (anti-quark) distribution functions. Functions $P_{ab}(z)$, where a and b are q or g, are splitting functions defined as:

$$\begin{aligned} P_{qq}(z) &= C_F\left[\tfrac{1+z^2}{(1-z)_+} + \tfrac{3}{2}\delta(1-z)\right], \quad P_{gq}(z) = C_F\tfrac{1+(1-z)^2}{z}, \\ P_{qg}(z) &= N_f[z^2+(1-z)^2], \\ P_{gg}(z) &= 2N_c\left[\tfrac{z}{(1-z)_+} + \tfrac{1-z}{z} + z(1-z)\right] + \tfrac{11N_c-2N_f}{6}\delta(1-z) \end{aligned} \tag{1.24}$$

where $C_F = \frac{N_c^2-1}{2N_c}$ and the "plus" prescription $u_+(z)$ is defined such that:

$$\int_0^1 dz u_+(z) f(z) = \int_0^1 dz u(z)(f(z)-f(1)) \tag{1.25}$$

The DGLAP equations Eq.(1.20) and Eq.(1.21) play a role as the renormalization group equations for the parton distribution functions with the renormalization scale Q^2. In fact, they are at leading-order (LO) since the integral kernels are given at the lowest order in α_s. The solution to the DGLAP equation is a systematic resummation of all powers of $(\alpha_s \ln Q^2)$.

Let us study the behavior of parton distribution functions at small x. In this regime, the relevant splitting functions are $P_{gq}(z)$ and $P_{gg}(z)$ since they are singular at small z:

$$P_{gq}(z) \approx \frac{2C_F}{z}, \quad P_{gg}(z) \approx \frac{2N_c}{z} \tag{1.26}$$

Consequently, the gluon distribution grows much faster than the quark distributions when x decreases. Therefore, one can neglect the evolution of quark distributions and, also, the quark contribution to the gluon distribution. Keeping the coupling constant α_s fixed for simplicity, the evolution equation for the gluon distribution is then:

$$\frac{\partial}{\partial \ln Q^2} G(x,Q^2) = \frac{\alpha_s}{2\pi}\int_x^1 \frac{dz}{z}\frac{2N_c}{z} G(\frac{x}{z},Q^2) \tag{1.27}$$

Doing a change of variable $z = x/\xi$ and integrating the equation with respect to $\ln Q^2$, one gets:

$$xG(x,Q^2) = xG_0(x,Q_0^2) + \frac{\alpha_s N_c}{\pi}\int_{Q_0^2}^{Q^2} d\ln Q'^2 \int_x^1 \frac{d\xi}{\xi}\xi G(\xi,Q'^2) \tag{1.28}$$

Taking the initial condition $G_0(\xi,Q_0^2) = \delta(\xi-1)$, which corresponds to one single gluon at Q_0^2, and solving the equation iteratively for $xG_n(x,Q^2)$ in the series solution $xG(x,Q^2) = xG_0(x,Q_0^2) + \sum_{n=1}^{\infty} xG_n(x,Q^2)$, one obtains:

$$xG_n(x,Q^2) = \sqrt{\bar{\alpha}\frac{\ln(Q^2/Q_0^2)}{\ln(1/x)}}\frac{\left(\bar{\alpha}\ln\frac{1}{x}\ln\frac{Q^2}{Q_0^2}\right)^{n-\frac{1}{2}}}{(n-1)!\,\Gamma(n+1)} \tag{1.29}$$

Resumming all such terms with the resummation parameter $\left(\bar{\alpha}\ln\frac{1}{x}\ln\frac{Q^2}{Q_0^2}\right)$, the solution of Eq.(1.28) for $x<1$ reads:

$$xG(x,Q^2) = \sqrt{\bar{\alpha}\frac{\ln(Q^2/Q_0^2)}{\ln(1/x)}} I_1\left[2\sqrt{\bar{\alpha}\ln\frac{1}{x}\ln\frac{Q^2}{Q_0^2}}\right] \tag{1.30}$$

where $\bar{\alpha} \equiv \frac{\alpha_s N_c}{\pi}$. This resummation is called the double logarithmic approximation (DLA). It predicts a rise in $xG(x,Q^2)$ when x decreases, which results in a rising quark distribution. Both rises in the gluon distribution and the quark distribution lead to an increase in the structure function $F_2(x,Q^2)$ at small x, which qualitatively agrees with the experimental data [25, 26].

1.4 BFKL evolution

The asymptotic behavior of the gluon distribution Eq. (1.30) is valid in the double logarithmic limit of small x and large Q^2. In case the longitudinal logarithm dominates the transverse logarithm, the resummation parameter now has just one logarithm of x, $\bar{\alpha}\ln\frac{1}{x}$, and the DLA becomes the leading logarithmic approximation (LLA). In this situation, one should study the $\frac{1}{x}$ evolution instead of the Q^2 evolution. This $\frac{1}{x}$ evolution was first formulated by Balitsky, Fadin, Kuraev and Lipatov (BFKL) [1–3]. Since the integration in Q^2 is now kept untouched, one can define the so-called unintegrated gluon distribution $f(x,k^2)$ as:

$$xG(x,Q^2) = \int_{Q_0^2}^{Q^2} d(\ln k^2) f(x,k^2) \tag{1.31}$$

The BFKL evolution equation for the unintegrated gluon distribution function, which is valid for sufficiently large transverse momenta, is then:

$$\frac{\partial f(x,k_\perp^2)}{\partial \ln(1/x)} = \frac{\bar{\alpha}}{\pi} \int \frac{d^2 l_\perp}{(k_\perp - l_\perp)^2} \left[f(x,l_\perp^2) - \frac{k_\perp^2}{2l_\perp^2} f(x,k_\perp^2) \right] \tag{1.32}$$

The eigenfunctions of the BFKL integral kernel are power functions of the form $f_\gamma(x,l_\perp^2) = (l_\perp^2/\Lambda^2)^{-\gamma}$ with eigenvalues $\bar{\alpha}\chi(\gamma)$, where Λ is some momentum scale and:

$$\chi(\gamma) = 2\psi(1) - \psi(\gamma) - \psi(1-\gamma) \tag{1.33}$$

with $\psi(\gamma) = \Gamma'(\gamma)/\Gamma(\gamma)$. The solution is then the linear combination of eigenfunctions:

$$f(x,k_\perp^2) = \int \frac{d\gamma}{2i\pi} c(\gamma) e^{\bar{\alpha}\chi(\gamma)\ln(1/x)} \left(\frac{k_\perp^2}{\Lambda^2}\right)^{-\gamma} \tag{1.34}$$

where the coefficient function $c(\gamma)$ is determined from the initial condition. Approximating the integral Eq.(1.34) at the saddle point value with $\gamma_{\text{saddle}} = 1/2$ and $\chi(\gamma_{\text{saddle}}) = 4\ln 2$, the leading small-$x$ behavior of the solution is then:

$$f(x,k_\perp^2) \sim \sqrt{\frac{\Lambda^2}{k_\perp^2}} \left(\frac{1}{x}\right)^{\alpha_P - 1} \tag{1.35}$$

where $\alpha_P - 1 = 4\bar{\alpha}\ln 2$. One can see that the growth of the gluon distribution function given by the BFKL evolution is much faster than that given by the DGLAP evolution (Eq.(1.30)).

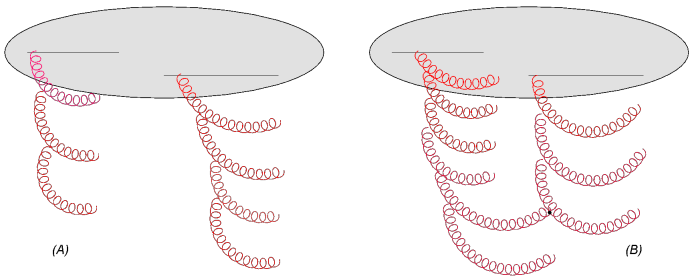

FIGURE 1.2: Gluon cascade in the proton wave function
(A) The BFKL cascade (linear evolution)
(B) The recombination effect (non-linear evolution)

The BFKL equation introduces an important step towards understanding asymptotically small-x regime of QCD. However, it raises some problems one of which we are going to address. As x decreases to very small values, the hadron - hadron cross section will eventually become so large that the unitarity bound is violated. Indeed, the parton density grows as x decreases, which leads to the overlapping of the partons' wave functions at some point. Hence, for such a dense system, one need to take into account the gluon recombination (Fig. 1.2), which should slow down and, then, saturate the rise of the gluon density. One attempt to solve the BFKL unitarity problem is of Gribov - Levin - Ryskin (GLR) [27] and Mueller - Qiu (MQ) [28] by introducing by hand the nonlinear term to the BKFL equation, which results in the GLR-MQ evolution equation. A systematic way of unitarizing the BFKL evolution is the Balisky - Kovchegov (BK) approach [4, 5] with the nonlinear BK evolution equation of following form:

$$\partial_Y T(k,Y) = \bar{\alpha} \int \frac{dl^2}{l^2} \left[\frac{l^2 T(l,Y) - k^2 T(k,Y)}{|k^2 - l^2|} + \frac{k^2 T(k,Y)}{\sqrt{4l^4 + k^4}} \right] - \bar{\alpha} T^2(k,Y) \tag{1.36}$$

where T is the dipole-nucleus scattering amplitude and l and k are transverse momenta. The discussion of the DGLAP and the BFKL evolutions couuld be summarized in Fig. 1.3, which illustrates the evolution of the parton distributions in different variables. The perturbative QCD regime is divided into two regions by the saturation scale: the linear evolution (DGLAP and BFKL) region and the saturation domain where the nonlinear correction is required. We will return to the BFKL and, also, the BK evolutions in the next chapter in the dipole formalism.

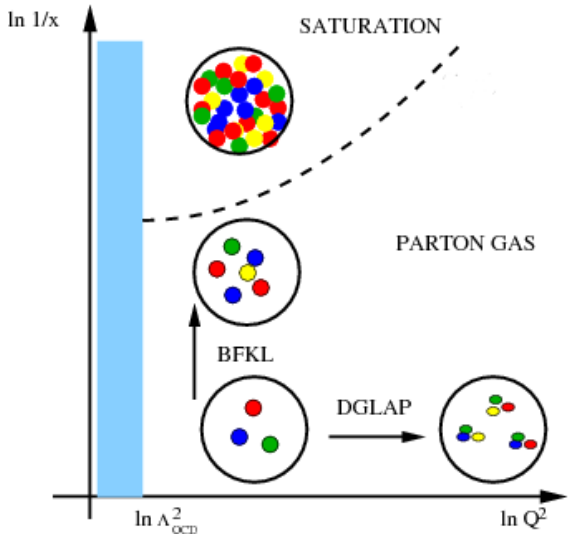

FIGURE 1.3: Different evolutions of the parton distributions.
(The dash curve shows the saturation scale $Q_s(x)$)

Chapter 2

Color Dipole Formulation

The modification of the hadronic wave function under the small-x evolution in the LLA requires to resum soft gluon emissions and virtual gluon corrections that bring powers of $\alpha_s \ln \frac{1}{x}$. This is a rather complicated job (see [29]). An elegant simplification is realized when taking advantage of the large-N_c limit in which gluons are replaced by color dipoles. The BFKL evolution is then the dipole evolution via the dipole branching and, hence, its derivation is relatively straightforward.
The aim of this chapter is to review the QCD evolution of onia at small-x in the dipole formalism developed by A. H. Mueller and collaborators [6–8, 30]. The evolution is generated by a kernel obtained from the construction of the light-cone wave function of onia in the large-N_c limit, where the gluons could be treated as color dipoles, which evolve independently of one another during the evolution.

2.1 Dipole formulation

2.1.1 Large N_c limit

The large N_c limit , which was introduced by 't Hooft [31], is the idea to take the limit $N_c \to \infty$ while keeping $\alpha_s N_c$ fixed, so that the small parameter in the problem becomes $\frac{1}{N_c}$. Recall the Fierz identity for $SU(N_c)$:

$$t^a_{ij} t^a_{kl} = \frac{1}{2}\left(\delta_{il}\delta_{jk} - \frac{1}{N_c}\delta_{ij}\delta_{kl}\right) \tag{2.1}$$

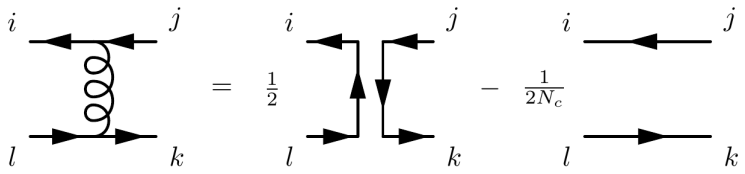

FIGURE 2.1: Graphical representation of the Fierz identity

where t^a $(a = 1, 2, \cdots, N_c^2 - 1)$ are generators of $SU(N_c)$ in the fundamental representation. The second term is suppressed in the large N_c limit and, hence, one can consider gluons as color dipoles (quark - anti-quark pairs). The effect of this consideration on the QCD vertices is shown in Fig. 2.2.
In the large-N_c limit, there is a significant simplification in the set of diagrams which contribute at leading $\frac{1}{N_c}$: only planar diagrams left. Let us consider, for example, diagrams in Fig. 2.3. Diagram (A) is the onium with an extra gluon (dipole): there are two color loops with two couplings and a factor of

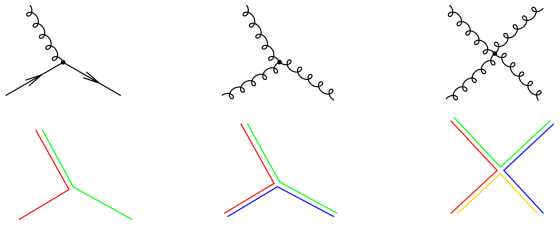

FIGURE 2.2: QCD vertices in dipole formalism

$1/N_c$ for average over colors, so that the overall factor is $(\alpha_s N_c)$; (B) has three color loops and fours coupling, which gives a factor of $(\alpha_s N_c)^2$. On the other hand, diagram (C) has only one color loop and still four couplings, which results in the contribution of order $(\alpha_s N_c)^2/N_c^2$. Therefore, this diagram will be suppressed compared to (A) and (B). The difference here is that, diagrams (A) and (B) are planar while (C) is not. Diagram (D) looks planar, but is also suppressed by $\frac{1}{N_c^2}$ as diagram (C), so it is effectively not. In summary, only planar diagrams give leading $1/N_c$ contribution.

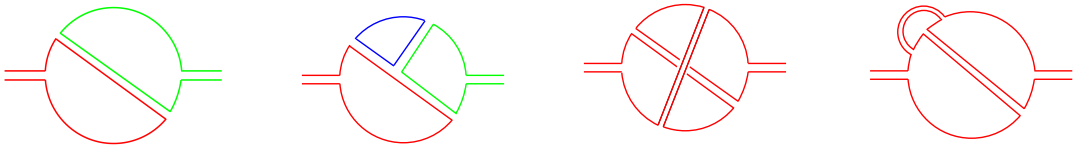

(A) (B) (C) (D)

FIGURE 2.3: Some example diagrams in the large N_c limit

2.1.2 The onium wave function

We are going to construct the onium light-cone wave function. Let us consider first the onium without soft gluons. The light-cone wave function is $\psi^{(0)}_{\alpha\beta}(k_{1\perp}, z_1)$ where α and β are quark and anti-quark spinor indices and $z_1 = k_{1+}/p_+$, p and k_1 are the momenta of the onium and the quark, respectively. In transverse coordinate space, the wave function is given by:

$$\psi^{(0)}_{\alpha\beta}(x_{01}, z_1) = \int \frac{d^2k_{1\perp}}{(2\pi)^2} e^{ik_{1\perp}\cdot x_{01}} \psi^{(0)}_{\alpha\beta}(k_{1\perp}, z_1) \tag{2.2}$$

where x_0 and x_1 are correspondingly transverse positions of the antiquark and the quark, and $x_{01} = x_1 - x_0$. The normalization is taken to be:

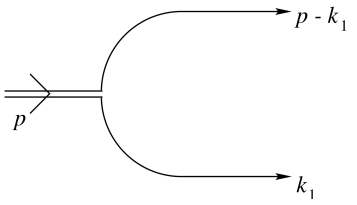

FIGURE 2.4: Onium wave function with no soft gluons [32]

$$\int \frac{d^2k_{1\perp}}{(2\pi)^2} \int_0^1 dz_1 \Phi^{(0)}(k_{1\perp}, z_1) = \int d^2x_{01} \int_0^1 dz_1 \Phi^{(0)}(x_{01}, z_1) = 1 \tag{2.3}$$

where:

$$\begin{aligned}\Phi^{(0)}(k_{1\perp},z_1) &= \sum_{\alpha\beta}|\psi^{(0)}_{\alpha\beta}(k_{1\perp},z_1)|^2\\ \Phi^{(0)}(x_{01},z_1) &= \sum_{\alpha\beta}|\psi^{(0)}_{\alpha\beta}(x_{01},z_1)|^2\end{aligned} \tag{2.4}$$

One now suppose that the onium emits a gluon at transverse position x_2 with momentum k_2. This emission could come from the quark or the anti-quark giving two contributions as shown in Fig. 2.5. Since we are interested in the high energy asymptotics, the momentum fraction of the gluon, $z_2 = k_{2+}/p_+$, is taken to be much smaller than z_1 and $1-z_1$, or the emitted gluon is soft.

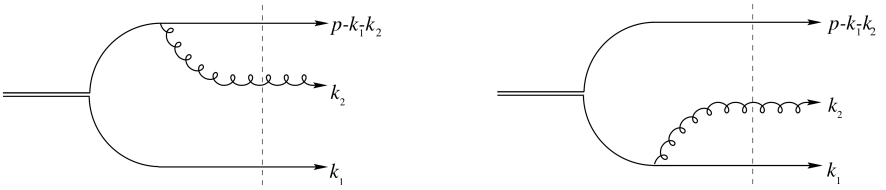

FIGURE 2.5: Onium wave function with one soft gluon [32]. The dashed line represents the point where the LCPT energy denominator is evaluated.

Using the LCPT rules, the onium wave function with one soft gluon in the light-cone gauge reads (see Appendix B):

$$\psi^{(1)a}_{\alpha\beta}(k_{1\perp},k_{2\perp};z_1,z_2) = 2g_s t^a\left[\psi^{(0)}_{\alpha\beta}(k_{1\perp},z_1)-\psi^{(0)}_{\alpha\beta}(k_{1\perp}+k_{2\perp},z_2)\right]\frac{k_{2\perp}\cdot\epsilon^\lambda_{2\perp}}{k^2_{2\perp}} \tag{2.5}$$

where the first term comes from the emission from the anti-quark (Fig. 2.5A) and the second term is from the quark (Fig. 2.5B), and ϵ^λ_2 is the polarization vector of the soft gluon with helicity λ. Although the form of the wave function in momentum space is relatively straightforward for one gluon emission, it is much more complicated when additional gluons present. For that reason, we employ the transverse coordinate representation of the wave function, which is obtained from the following Fourier transform:

$$\psi^{(1)a}_{\alpha\beta}(x_{01},x_{02};z_1,z_2) = \int\frac{d^2k_{1\perp}d^2k_{2\perp}}{(2\pi)^4}e^{ik_{1\perp}\cdot x_{01}+ik_{2\perp}\cdot x_{02}}\psi^{(1)a}_{\alpha\beta}(k_{1\perp},k_{2\perp};z_1,z_2) \tag{2.6}$$

where x_2 is the transverse position of the soft gluon, and $x_{ij} = x_j - x_i$. Substituting Eq.(2.5) into Eq.(2.6), one finds:

$$\psi^{(1)a}_{\alpha\beta}(x_{01},x_{02};z_1,z_2) = \frac{ig_s t^a}{\pi}\psi^{(0)}_{\alpha\beta}(x_{01},z_1)\left(\frac{x_{02}}{x^2_{02}}-\frac{x_{12}}{x^2_{12}}\right)\cdot\epsilon^\lambda_{2\perp} \tag{2.7}$$

The square of the wave function takes the form:

$$\Phi^{(1)}(x_{01},z_1) = \frac{1}{2\pi}\int d^2x_2\int_{z_0}^{z_1}\frac{dz_2}{2z_2}\sum_{a\lambda\alpha\beta}|\psi^{(1)a}_{\alpha\beta}(x_{01},x_{02};z_1,z_2)|^2 \tag{2.8}$$

where we have put a lower cut-off z_0 on the z_2 - integral. Using the explicit form of $\psi^{(1)a}_{\alpha\beta}(x_{01},x_{02};z_1,z_2)$ in Eq.(2.7), we gets:

$$\Phi^{(1)}(x_{01},z_1) = \int d^2x_2\int_{z_0}^{z_1}\frac{dz_2}{z_2}\frac{\alpha_s N_c}{2\pi^2}\frac{x^2_{01}}{x^2_{02}x^2_{12}}\Phi^{(0)}(x_{01},z_1) \tag{2.9}$$

where C_F is replaced by $N_c/2$ in the large-N_c limit. We see that in this form, the soft gluon emission factorizes from the onium wave function with no soft gluon.

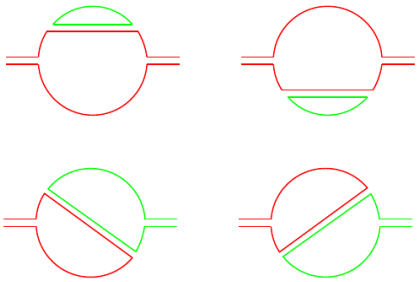

FIGURE 2.6: Color structure of the onium wave function with one soft gluon

The integral kernel in Eq.(2.9) could be decomposed as:

$$\frac{\alpha_s N_c}{2\pi^2}\frac{x_{01}^2}{x_{02}^2 x_{12}^2} = \frac{\alpha_s N_c}{2\pi^2}\left(\frac{1}{x_{12}^2} + \frac{1}{x_{02}^2} - \frac{2x_{02}\cdot x_{12}}{x_{02}^2 x_{12}^2}\right) \tag{2.10}$$

The first two terms correspond to two upper diagrams in Fig. 2.6, while the third term is the interference term coming from two remaining lower diagrams. When adding another soft gluon into the onium wave function, there appears two types of diagrams: planar and non-planar. Since the non-planar diagrams (see Fig. 2.3C) are neglected in the large-N_c limit, we are left with the planar ones (see Fig. 2.3B). In fact, the non-planar diagrams are due to the coherent emission from the $q\bar{q}$ pair. Therefore, the neglection of those means once the original dipole has emitted one soft gluon, it effectively emits no more gluons. Consequently, in the large-N_c limit, the emission of one soft gluon at x_k off a dipole x_{ij} after rapidity dy is equivalent to the splitting of the original color dipole into two subsequent color dipoles x_{ik} and x_{jk} with the probability:

$$dP(x_{ij} \to x_{ik}, x_{jk}) = \bar{\alpha} dY \frac{d^2x_k}{2\pi}\frac{x_{ij}^2}{x_{ik}^2 x_{jk}^2} \tag{2.11}$$

where the rapidity $Y = \ln\frac{1}{z}$ (at high energy) and $\bar{\alpha} \equiv \frac{\alpha_s N_c}{\pi}$. The splitting will be iterated to the end of the evolution and, hence, the evolution in rapidity is essentially the sequence of independent decays of dipoles into pairs dipoles creating dipole cascade.

2.2 BFKL evolution in the dipole formalism

As realized in the end of the previous section, the dipole branching is a stochastic process. It means that the number of dipoles of a certain size at rapidity Y fluctuates event by event. Let us define $n(r_\perp, Y|x_{01})$ as the mean number of dipoles (averaged over events) of size larger than $r_\perp$ at rapidity Y from the original dipole x_{01}. At the rapidity $Y + dY$, the mean number $n(r_\perp, Y + dY|x_{01})$ has two contributions (Fig. 2.7). In case the original dipole x_{01} splits into two dipoles x_{02} and x_{12} after rapidity dY, the contribution comes from the mean numbers of dipoles $n(r_\perp, Y|x_{02})$ and $n(r_\perp, Y|x_{12})$ of two daughter. On the other hand, if the original dipole is retained after dY then $n(r_\perp, Y|x_{01})$ will contribute. As a result, one has:

$$\begin{aligned} n(r_\perp, Y + dY|x_{01}) = &\int dP(x_{01} \to x_{02}, x_{12})\left[n(r_\perp, Y|x_{02}) + n(r_\perp, Y|x_{12})\right] \\ &+ \left(1 - \int dP(x_{01} \to x_{02}, x_{12})\right) n(r_\perp, Y|x_{01}) \end{aligned} \tag{2.12}$$

After being rearranged, the equation above becomes:

$$\partial_Y n(r_\perp, Y|x_{01}) = \bar{\alpha}\int \frac{d^2x_2}{2\pi}\frac{x_{01}^2}{x_{02}^2 x_{12}^2}\left[n(r_\perp, Y|x_{02}) + n(r_\perp, Y|x_{12}) - n(r_\perp, Y|x_{01})\right] \tag{2.13}$$

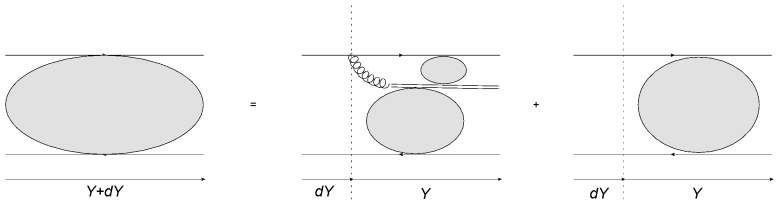

FIGURE 2.7: Graphical illustration of the BFKL equation

This is the BFKL evolution equation in the transverse coordinate space in the dipole formalism (see [13]). The action of the BFKL kernel K on a function n of the transverse vector x_{01} is defined as:

$$K \otimes n(x_{01}) = \bar{\alpha} \int \frac{d^2x_2}{2\pi} \frac{x_{01}^2}{x_{02}^2 x_{12}^2} \left[n(x_{02}) + n(x_{12}) - n(x_{01}) \right] \tag{2.14}$$

Eigenfunctions of the BFKL kernel are power functions of the form:

$$n_\gamma(r_\perp, Y | x_{01}) = \left(\frac{x_{01}^2}{r_\perp^2} \right)^\gamma \tag{2.15}$$

with eigenvalues $\bar{\alpha}\chi(\gamma)$, where $\chi(\gamma)$ is given in Eq.(1.33) since the kernels are just the Fourier transform of each other. The general solution is then the linear combination of the eigenfunctions Eq.(2.15), which reads:

$$n(r_\perp, Y | x_{01}) = \int \frac{d\gamma}{2\pi i} f(\gamma) e^{\bar{\alpha} Y \chi(\gamma)} \left(\frac{x_{01}^2}{r_\perp^2} \right)^\gamma \tag{2.16}$$

Taking the initial condition so that coefficient function $f(\gamma) = \frac{1}{\gamma}$, then:

$$n(r_\perp, Y | x_{01}) = \int \frac{d\gamma}{2\pi i \gamma} \exp\left(\bar{\alpha} Y \chi(\gamma) + \gamma \ln \frac{x_{01}^2}{r_\perp^2} \right) \tag{2.17}$$

For Y large, the saddle-point is at $\gamma_s \simeq \frac{1}{2}$. The mean number of dipoles in the saddle-point approximation is then

$$n(r_\perp, Y | x_{01}) \simeq \exp\left(\bar{\alpha} Y \chi(\frac{1}{2}) + \frac{1}{2} \ln \frac{x_{01}^2}{r_\perp^2} \right) \simeq \frac{x_{01}}{r_\perp} e^{\bar{\alpha} Y 4 \ln 2} \tag{2.18}$$

This is nothing but the result we obtained in the previous chapter (Eq.(1.35)).

2.3 Balisky - Kovchegov equation

We now consider the scattering of an onium x_{01} off a nucleus A at some fixed impact parameter. The onium is supposed to be boosted to rapidity Y while the nucleus is at rest, so that all evolution is now in the onium. Let us define $S(x_{01}, Y)$ as the S-matrix element of the scattering.

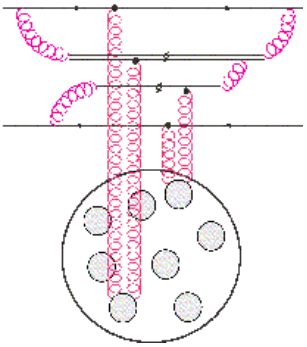

FIGURE 2.8: Onium - nucleus scattering

$S(x_{01}, Y)$ could be interpreted as the probability amplitude that there is no interaction between the original dipole x_{01} and the target at rapidity Y. In one step dY of the evolution, either the original dipole splits into two dipoles x_{02} and x_{12} and the S-matrix would be given by $S(x_{01}, Y + dY) = S(x_{02}, Y)S(x_{12}, Y)$, or it does not split so that $S(x_{01}, Y + dY) = S(x_{01}, Y)$. Summing up those two contributions weighted by their respective probabilities, one gets:

$$S(x_{01}, Y + dY) = \int dP(x_{01} \to x_{02}, x_{12}) S(x_{02}, Y) S(x_{12}, Y) + \left(1 - \int dP(x_{01} \to x_{02}, x_{12})\right) S(x_{01}, Y) \tag{2.19}$$

Using the explicit form of $dP(x_{01} \to x_{02}, x_{12})$ in Eq.(2.11), we obtain:

$$\partial_Y S(x_{01}, Y) = \bar{\alpha} \int \frac{d^2 x_2}{2\pi} \frac{x_{01}^2}{x_{02}^2 x_{12}^2} \left[S(x_{02}, Y) S(x_{12}, Y) - S(x_{01}, Y)\right] \tag{2.20}$$

Instead of $S(x_{01}, Y)$, we define the forward onium-nucleus scattering amplitude $N(x_{01}, Y)$ as $N(x_{01}, Y) = 1 - S(x_{01}, Y)$. The evolution equation for $N(x_{01}, Y)$ is then:

$$\partial_Y N(x_{01}, Y) = \bar{\alpha} \int \frac{d^2 x_2}{2\pi} \frac{x_{01}^2}{x_{02}^2 x_{12}^2} \left[N(x_{02}, Y) + N(x_{12}, Y) - N(x_{01}, Y) - N(x_{02}, Y) N(x_{12}, Y)\right] \tag{2.21}$$

This is the Balisky - Kovchegov (BK) evolution equation [4, 5]. The initial condition for the BK evolution is taken to be the McLerran - Venugopalan (MV) amplitude []

$$N_{MV}(x_{01}, Y = 0) = 1 - \exp\left\{-\frac{x_{01}^2 Q_{MV}^2}{4} \ln\left(e + \frac{4}{x_{01}^2 \Lambda_{QCD}^2}\right)\right\} \tag{2.22}$$

where Λ_{QCD} is the QCD scale and Q_{MV} is the momentum scale characterized for the nucleus. The BK equation is similar to a diffusion equation with a growth and a saturation term. The linear part of the BK equation is nothing but the BFKL equation, which gives an exponential rise of N with the rapidity due to the dipole branching. When the amplitude approach the fixed point, $N \sim 1$, the nonlinear term becomes important which would cause the evolution to be slowed down and, then saturated. Thus, this term behaves as a unitarity - preserving term, which ensures that $N \leq 1$ during the evolution.

For asymptotically large Y, due to the unitarity-preserving effect, the solution to the BK equation converges to a traveling wave, which is a smooth function of the dipole size x_{01} connecting 0 and 1 at fixed Y, and the evolution in Y is just a translation in x_{01} [33]. The transition to the saturation region occurs at some scale $R_s(Y) = 2/Q_s(Y)$, where $Q_s(Y)$ is the saturation momentum, defined, for example, by:

$$N(x_{01} = R_s(Y), Y) = \frac{1}{2} \tag{2.23}$$

For N around the transition region, $N \ll 1$, the solution can be obtained by solving the branching-diffusion equation with a moving boundary [33, 34], which reads:

$$N(x_{01}, Y) = c_N \ln \frac{1}{x_{01}^2 Q_s^2(Y)} \left[x_{01}^2 Q_s^2(Y)\right]^{\gamma_0} \exp\left\{-\frac{\ln^2[x_{01}^2 Q_s^2(Y)]}{2\bar{\alpha} Y \chi''(\gamma_0)}\right\} \tag{2.24}$$

where c_N is a constant and γ_0 solves the equation $\chi(\gamma_0)/\gamma_0 = \chi'(\gamma_0)$. The asymptotic form of the saturation momentum at large Y reads:

$$Q_s^2(Y) = Q_{MV}^2 \frac{e^{\bar{\alpha} Y \chi'(\gamma_0)}}{(\bar{\alpha} Y)^{3/2\gamma_0}} \tag{2.25}$$

An important feature of Eq.(2.24) is that $N \sim e^{\gamma_0 x}$, with $x = \ln\left[x_{01}^2 Q_s^2(Y)\right]$. This shape does not depend on the details of the initial condition, provided that the initial condition is steep enough, namely

$N(Y=0) \sim e^{\beta x}$ with $\beta > \gamma_0$. Eq.(2.24) valid in the so-called scaling region which is defined as the region in which N effectively becomes a function of the single scaling variable $x_{01}^2 Q_s^2(Y)$ only. In the scaling region, x_{01} obeys the following inequality:

$$1 < |\ln[x_{01}^2 Q_s^2(Y)]| \leq \sqrt{\bar{\alpha} Y \chi''(\gamma_0)} \tag{2.26}$$

Fig. 2.9 shows a numerical solution to the BK equation with fixed coupling for several values of the rapidity Y. One can see from this figure that the nonlinear evolution pushes the dipole amplitude N towards lower values of x_{01} as Y increases.

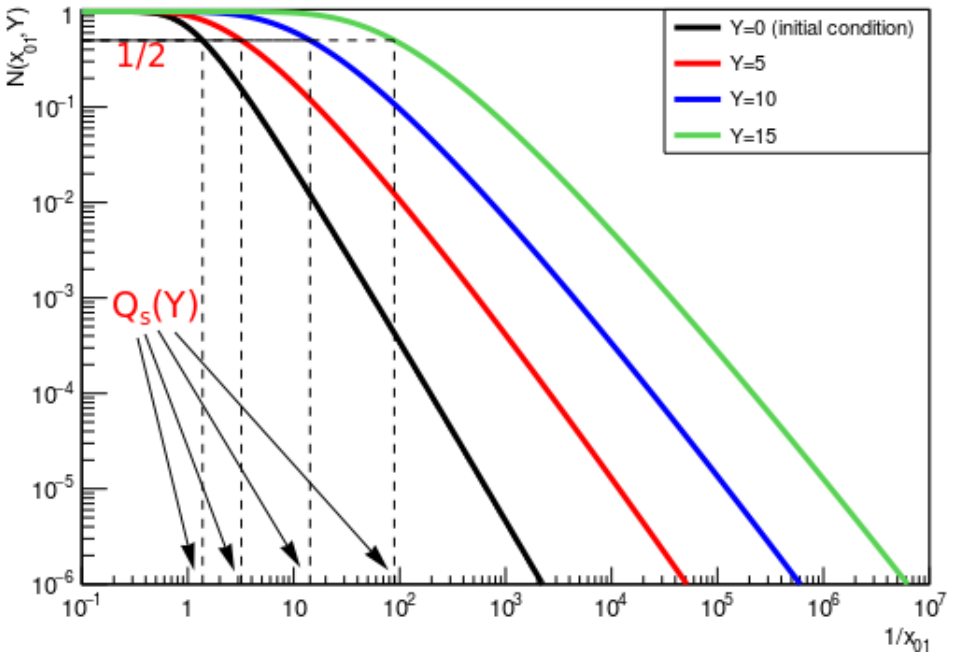

FIGURE 2.9: Solution of the BK equation at fixed coupling

Chapter 3

Diffractive dissociation in onium - nucleus scattering

This chapter is deserved for presenting the main results of the internship. Here we will present an analogy between the diffractive virtual photon (onium) - nucleus scattering and the ancestry problem in the dipole evolution. A reference to the one - dimensional branching random walk process will be also mentioned.

3.1 Diffractive dissociation in DIS

3.1.1 Picture of diffractive dissociation

In the $\gamma^* A$ scattering, the interaction is classified by the characteristics of the final states. In elastic events, the particles in the final state are the same as the ones in the initial state, and only their momenta are redistributed. Diffractive scattering is referred to a process in which the virtual photon interacts with the target producing a number of hadrons in the final state while the target is kept intact and generating a rapidity gap, which is defined as a region in rapidity around the nucleus with no particle observed. This corresponds to, at high energy, an angular gap in detectors of colliding experiments.

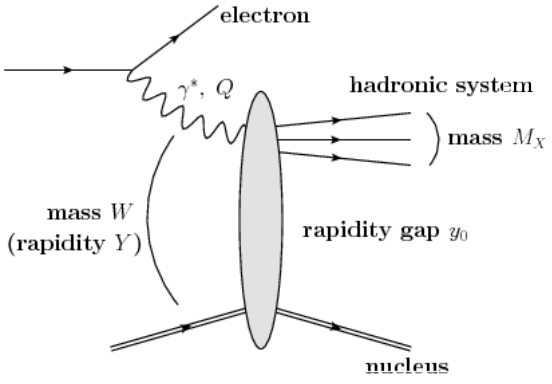

FIGURE 3.1: Graphical illustration of the diffractive scattering

The diffractive scattering is illustrated in Fig. 3.1. We denote the virtuality of the photon by Q, and the center of mass energy (the total mass of the final state at rapidity Y) of the $\gamma^* A$ scattering by W. The produced hadronic system, which is denoted by X with total invariant mass M_X, leaves a rapidity gap y_0 between the target and the slowest produced hadron. It fills in the rapidity range $\tilde{y}_0 = \ln[\left(M_X^2 + Q^2\right)/Q^2]$, while the net rapidity interval is $Y = \ln[(W^2 + Q^2)/Q^2]$. Therefore, the rapidity

gap is given by $y_0 = Y - \tilde{y}_0$.

The diffraction in DIS could be classified as low-mass and high-mass diffraction based on the value of M_X. When the net invariant mass of the produced hadrons is small, $M_X \ll Q$ (low-mass), the rapidity gap covers much of the total rapidity, $y_0 \approx Y$. On the other hand, when $M_X \gg Q$ (high-mass), the rapidity gap may be still large but the filled rapidity range is large as well.

In high energy scattering, it is possible to choose a reference frame in which the virtual photon is fast enough to almost always convert to a pair of quark-anti-quark (onium) whose size is unchanged during the scattering. Therefore, the virtual photon - nucleus interaction is corresponding to the onium - nucleus interaction. Consequently, one can use the QCD dipole evolution scenario to examine the DIS diffractive events.

3.1.2 Quantitative evaluation of the diffractive cross section

We are now moving on to the quantitative predictions of the diffraction from the interpretation of the BK equation. In the rest frame of the nucleus, the onium carries the full rapidity Y and, hence, does not interact with the nucleus as a bare $q\bar{q}$ dipole state, but as a highly evolved quantum state represented by a set of dipoles. The evolution of the onium is stochastic, namely its quantum state differs from one event to another event. The scattering amplitude $N(x_{01}, Y)$ is then related to the probability $P(x_{01}, \tilde{y} = Y | R = 1/Q_{MV})$ to have at least one dipole in the onium Fock state at rapidity Y whose size is larger than $1/Q_{MV}$. The probability $P(x_{01}, \tilde{y}|R)$ solves the BK equation:

$$\partial_{\tilde{y}} P(x_{01}, \tilde{y}|R) = \bar{\alpha} \int \frac{d^2x_2}{2\pi} \frac{x_{01}^2}{x_{02}^2 x_{12}^2} \left[P(x_{02}, \tilde{y}|R) + P(x_{12}, \tilde{y}|R) - P(x_{01}, \tilde{y}|R) - P(x_{02}, \tilde{y}|R) P(x_{12}, \tilde{y}|R) \right] \tag{3.1}$$

with the initial condition to be the Heaviside distribution:

$$P(x_{01}, \tilde{y} = 0|R) = \theta \left(\ln \frac{x_{01}^2}{R} \right) \tag{3.2}$$

This initial condition is different from the initial condition for the amplitude N, which is taken to be the MV amplitude. However, in the large-rapidity asymptotics, solutions of P and N fall into the same universality class, which enables following identification:

$$P(x_{01}, Y|1/Q_{MV}) \simeq N(x_{01}, Y) \tag{3.3}$$

We now return to the diffraction problem. The onium size x_{01} is supposed to be small compared to $1/Q_s(Y)$, namely the onium is far from the saturation region of nucleus. In this regime, the elastic cross section, which is of first order in N, will dominate the total cross section. Let us put the rapidity $\tilde{y}_0 \gg 1$ on onium (highly-evolved onium state), while the rapidity of the nucleus is $y_0 = Y - \tilde{y}_0$, with Y to be the total rapidity. The condition for the whole partonic system to scatter elastically with the nucleus with a significant probability is that there is at least one dipole in the onium Fock state at the rapidity $\tilde{y}_0$ crossing the nuclear saturation boundary and, hence, absorbed by the target. This is equivalent to the existence of at least one exceptionally large dipole of size greater than the saturation scale $1/Q_s(y_0)$ in the highly-evolved quantum state of the onium. This results in a diffractive event with a rapidity gap of size y_0. Therefore, it is allowed to identify the rapidity gap distribution to the probability $P(x_{01}, \tilde{y}_0|1/Q_s(y_0))$:

$$\frac{d\sigma_{\text{diff}}}{dy_0} = P(x_{01}, \tilde{y}_0|1/Q_s(y_0)) \tag{3.4}$$

The exceptionally large dipoles which are necessary for a diffractive event are generated by two types of fluctuations in the onium evolution [36, 37]. In the early stage of the evolution, there are only a few dipoles and, thus, the state is subject to fluctuations which strongly determine the largest size of dipoles,

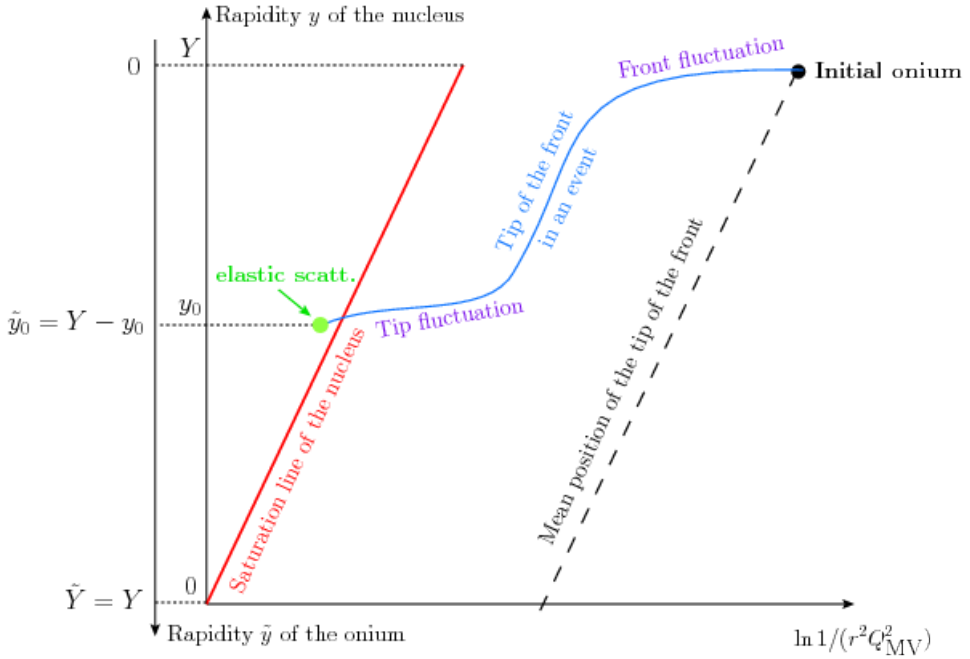

FIGURE 3.2: Schematic picture of a diffractive event with rapidity gap of size y_0. The vertical downward axis is the rapidity of the onium, while the upward one is of the nucleus. The saturation line of the nucleus is shown by the red continuous line together with the position of the tip of the front in a particular event (curly continuous line). The combination of the front fluctuation and the tip fluctuation produces unusually large dipoles comparing to the mean position of the tip (dashed line) [35]

which is called position of the tip of the front, at later rapidities. This type of fluctuations is referred as the front fluctuations. Fluctuations may also be exhibited at the tip of the front, which is then called tip fluctuations. Those fluctuations together create a few exceptionally large dipoles around rapidity y_0. As discussed above, $P(x_{01}, \tilde{y}_0 | 1/Q_s(y_0))$ solves the BK equation. Therefore, for large rapidity, the diffractive cross section in the scaling region reads:

$$\frac{d\sigma_{\rm diff}}{dy_0} = c_{\rm diff} \left[x_{01}^2 \tilde{Q}_s^2(\tilde{y}_0)\right]^{\gamma_0} \ln \frac{1}{x_{01}^2 \tilde{Q}_s^2(\tilde{y}_0)} \exp\left\{-\frac{\ln^2\left[x_{01}^2 \tilde{Q}_s^2(\tilde{y}_0)\right]}{2\bar{\alpha}\tilde{y}_0 \chi''(\gamma_0)}\right\} \tag{3.5}$$

where $c_{\rm diff}$ is an unknown constant and the momentum $\tilde{Q}_s$ is defined as:

$$\tilde{Q}_s^2(\tilde{y}_0) = Q_s^2(y_0) \frac{e^{\bar{\alpha}\tilde{y}_0 \chi'(\gamma_0)}}{(\bar{\alpha}\tilde{y}_0)^{3/2\gamma_0}} \tag{3.6}$$

We now assume that:

$$\ln\left[x_{01}^2 Q_s^2(Y)\right] \gg \ln\left[\frac{\bar{\alpha}Y}{\bar{\alpha}y_0\bar{\alpha}(Y-y_0)}\right] \tag{3.7}$$

which means the rapidity gap y_0 is not close to 0 and Y. From this condition, one has:

$$\ln\left[x_{01}^2 \tilde{Q}_s^2(\tilde{y}_0)\right] = \ln\left[x_{01}^2 Q_s^2(Y) \left(\frac{\bar{\alpha}Y}{\bar{\alpha}y_0\bar{\alpha}(Y-y_0)}\right)^{3/2\gamma_0}\right] \simeq \ln\left[x_{01}^2 Q_s^2(Y)\right] \tag{3.8}$$

The equation Eq. (3.5) then can be rewritten as:

$$\frac{d\sigma_{\rm diff}}{dy_0} = c_{\rm diff} \left[\frac{\bar{\alpha}Y}{\bar{\alpha}y_0\bar{\alpha}(Y-y_0)}\right]^{3/2} \exp\left\{-\frac{\ln^2\left[x_{01}^2 Q_s^2(Y)\right]}{2\bar{\alpha}\tilde{y}_0 \chi''(\gamma_0)}\right\} \times \left[x_{01}^2 Q_s^2(Y)\right]^{\gamma_0} \ln \frac{1}{x_{01}^2 Q_s^2(Y)} \tag{3.9}$$

Going deep into the scaling region, one can neglect the exponential suppression. The y_0-independent term in Eq.(3.9) is then the total cross section up to a constant $c_{\rm tot}$, hence,

$$\frac{1}{\sigma_{\rm tot}}\frac{d\sigma_{\rm diff}}{dy_0} = \frac{c_{\rm diff}}{c_{\rm tot}}\left[\frac{\bar{\alpha}Y}{\bar{\alpha}y_0\bar{\alpha}(Y-y_0)}\right]^{3/2} \tag{3.10}$$

This is the result obtained in [35, 38]. The overall constant is unknown in the theory.
We are now going to formulate the ancestry problem of the parton evolution and explain how it is related to the diffraction problem in the high-energy onium - nucleus scattering.

3.2 Ancestry problem and its analogy to the diffraction

3.2.1 Ancestry problem in partonic evolution

As discussed in the previous chapter, since the initial dipole size is chosen in such a way that the mean position of the tip of the front is far enough from the saturation boundary of the nucleus, diffractive events are then due to rare fluctuations to a few unusually large dipoles in the evolution. Those boundary dipoles come from a most recent common ancestor at rapidity $\tilde{y}_0$ (of the onium). In other words, at the rapidity $\tilde{y}_0$ of the onium, the rare fluctuations occur and generate a dipole with unusually large size, and some of its offsprings cross the boundary of the nucleus at the end of the evolution(see Fig. 3.3), which creates a diffractive event. Therefore, the distribution of the rapidity gap y_0 in diffractive events is equivalent to the rapidity distribution of the most recent common ancestor of few largest dipoles at the end of the evolution.

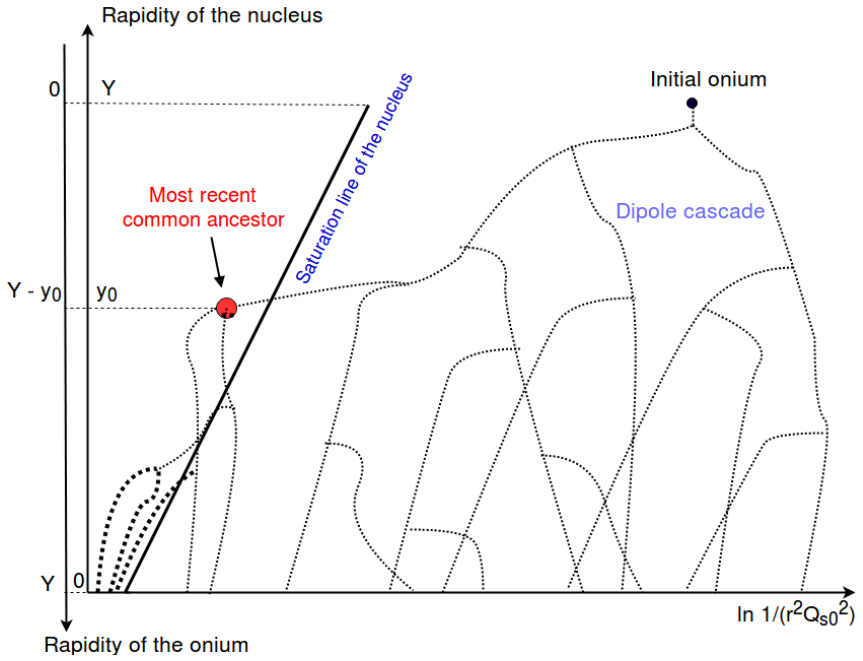

FIGURE 3.3: Schematic illustration of the ancestry problem. The dot lines represent the dipole evolution in rapidity. There are three (rightmost) dipoles in this realization illustrated to cross the saturation boundary of the nucleus at the end of the dipole evolution. Their most recent common ancestor is at the rapidity $Y - y_0$ (red dot) and splits to large fluctuations. The curly continuous line shows the saturation scale of the nucleus.

Let us define $\mathcal{G}(x_{01}, Y, y_0)$ to be the probability distribution of the rapidity y_0 at which the most recent common ancestor of all dipoles of size larger than $1/Q_s(y_0)$ split, and $\mathcal{U}(x_{01}, Y)$ to be the probability that there is no dipole in the state of the onium evolved to the rapidity Y whose size is larger than $1/Q_s(y_0)$.

The probability $\mathcal{U}(x_{01}, Y)$ then solves the ordinary BK equation:

$$\partial_Y \mathcal{U}(x_{01}, Y) = \bar{\alpha} \int \frac{d^2x_2}{2\pi} \frac{x_{01}^2}{x_{02}^2 x_{12}^2} \left[\mathcal{U}(x_{02}, Y)\mathcal{U}(x_{12}, Y) - \mathcal{U}(x_{01}, Y)\right] \tag{3.11}$$

The initial condition for $\mathcal{U}$ is the Heaviside distribution function:

$$\mathcal{U}(x_{01}, Y = 0) = \theta\left(\ln x_{01}^2 Q_{MV}^2\right) \tag{3.12}$$

We are now at the position to establish the evolution equation for $\mathcal{G}(x_{01}, Y, y_0)$. In a rapidity step dY of the evolution, the parent dipole may emit a real gluon, namely split into two dipoles; then the most recent common ancestor of the unusual large dipoles will be from one of two daughter dipoles, while the remainder contains no dipole whose size is larger the than the inverse of the saturation scale of the nucleus. On the other hand, the initial dipole is unchanged (no real gluon emission) and, certainly, contains the most recent common ancestor. Consequently, $\mathcal{G}(x_{01}, Y, y_0)$ obeys the following equation:

$$\begin{aligned} \mathcal{G}(x_{01}, Y + dY, y_0) = \bar{\alpha} dY \int \frac{d^2x_2}{2\pi} \frac{x_{01}^2}{x_{02}^2 x_{12}^2} \left[\mathcal{G}(x_{02}, Y, y_0)\mathcal{U}(x_{12}, Y) + \mathcal{G}(x_{02}, Y, y_0)\mathcal{U}(x_{12}, Y)\right] \\ + \left(1 - \bar{\alpha} dY \int \frac{d^2x_2}{2\pi} \frac{x_{01}^2}{x_{02}^2 x_{12}^2}\right) \mathcal{G}(x_{01}, Y, y_0) \end{aligned} \tag{3.13}$$

After being rearranged, the evolution equation for the distribution $\mathcal{G}(x_{01}, Y, y_0)$ becomes:

$$\partial_Y \mathcal{G}(x_{01}, Y, y_0) = \bar{\alpha} \int \frac{d^2x_2}{2\pi} \frac{x_{01}^2}{x_{02}^2 x_{12}^2} \left[\mathcal{G}(x_{02}, Y, y_0)\mathcal{U}(x_{12}, Y) + \mathcal{G}(x_{02}, Y, y_0)\mathcal{U}(x_{12}, Y) - \mathcal{G}(x_{01}, Y, y_0)\right] \tag{3.14}$$

The initial condition for $\mathcal{G}$ is taken to be:

$$\mathcal{G}(x_{01}, Y = y_0, y_0) = \bar{\alpha} \int \frac{d^2x_2}{2\pi} \frac{x_{01}^2}{x_{02}^2 x_{12}^2} \left(1 - \mathcal{U}(x_{02}, y_0)\right) \left(1 - \mathcal{U}(x_{12}, y_0)\right) \tag{3.15}$$

which comes from the fact that the unusually large dipoles are from the most recent common ancestor at the rapidity $\tilde{y}_0$.

A similar problem for one-dimensional branching random walks (BRW) has been discussed recently by B. Derrida and P. Mottishaw [39] in the framework of Generalized Random Energy Model (GREM). Suppose there is a branching random walk process in x direction and in time t starting with a single particle at $t = 0$ which obeys the branching-diffusion equation $\partial_t n(x, t) = \chi(\partial_x) \cdot n(x, t)$. The second-order differential kernel χ has eigenfunctions of the form $e^{\gamma x}$ and corresponding eigenvalues $\chi(\gamma)$. After a large time t, let us pick exactly two leftmost particles and look for their most recent common ancestor splitting time $t - t_0$. Derrida and Mottishaw showed that the distribution of t_0 obeys the law:

$$P(t_0) = \frac{1}{\gamma_0} \frac{1}{\sqrt{2\pi\chi''(\gamma_0)}} \left[\frac{t}{t_0(t - t_0)}\right]^{3/2} \tag{3.16}$$

where γ_0 solves $\chi'(\gamma_0) = \chi(\gamma_0)/\gamma_0$. This distribution is similar to Eq.(3.10) up to a constant and some identifications. This implies there could be an underlying relation between two problems, and once this relation is addressed, the overall constant in Eq.(3.10) could be determined theoretically.

In the following, we will relate the equation for the ancestry problem Eq.(3.14) to the so-called Kovchegov - Levin equation describing high-mass diffraction.

3.2.2 Kovchegov - Levin equation and ancestry problem

Good and Walker [40] provided an elegant picture to describe the diffractive dissociation, in which diffraction is proportional to the dispersion in cross sections for the diagonal channels of the scattering. Employing the Good and Walker picture, A. H. Mueller and S. Munier [35] obtained the following equation

for the high-mass diffractive cross section $\sigma_{\rm diff}$ at fixed impact parameter:

$$\sigma_{\rm diff} = \left\langle \prod_k \left[S(r_k, y_0)\right]^2 \right\rangle_{x_{01}, \tilde{y}_0 = Y - y_0} - \left\langle \prod_k S(r_k, y_0) \right\rangle^2_{x_{01}, \tilde{y}_0 = Y - y_0} \tag{3.17}$$

where $S(r, y)$ solves the BK equation for the S-matrix element corresponding to the forward scattering of a dipole of size r at rapidity y off the nucleus, and the notation $\langle \cdots \rangle_{x_{01}, \tilde{y}}$ is denoted for the average over all realizations of the Fock state of the onium of initial size x_{01} at the rapidity $\tilde{y}$ (namely, over all events). The products in Eq.(3.17) are taken over all dipoles in the onium wave function. We realize that the second term in Eq.(3.17) is independent of y_0 as a consequence of the Lorentz boost invariant. Hence, the distribution of the rapidity gap is given by:

$$\frac{d\sigma_{\rm diff}}{dy_0} = -\frac{\partial}{\partial y_0} S_2(x_{01}, Y - y_0) \tag{3.18}$$

where we have introduced the notation:

$$S_2(x_{01}, \tilde{y}) \equiv \left\langle \prod_k \left[S(r_k, y_0)\right]^2 \right\rangle_{x_{01}, \tilde{y}} \tag{3.19}$$

The evolution of S_2 is governed by the BK equation of the form:

$$\partial_{\tilde{y}} S_2(x_{01}, \tilde{y}) = \bar{\alpha} \int \frac{d^2 x_2}{2\pi} \frac{x_{01}^2}{x_{02}^2 x_{12}^2} \left[S_2(x_{02}, \tilde{y}) S_2(x_{12}, \tilde{y}) - S_2(x_{01}, \tilde{y})\right] \tag{3.20}$$

with the initial condition:

$$S_2(x_{01}, \tilde{y} = 0) = \left[S(x_{01}, y_0)\right]^2 \tag{3.21}$$

The S-matrix element S, as mentioned before, solves the BK equation Eq.(2.20) with the initial condition taken to be the MV amplitude. The equation Eq.(3.20) is first derived by Y. V. Kovchegov and E. Levin [41] (see also [13]), which is known as the Kovchegov - Levin (nonlinear) evolution equation.
Differentiating the equation Eq.(3.20) with respect to y_0, one can get:

$$\begin{aligned} \partial_{\tilde{y}} \left(-\frac{\partial S_2(x_{01}, \tilde{y})}{\partial y_0} \right) = \bar{\alpha} \int \frac{d^2 x_2}{2\pi} \frac{x_{01}^2}{x_{02}^2 x_{12}^2} \Bigg[\left(-\frac{\partial S_2(x_{02}, \tilde{y})}{\partial y_0} \right) S_2(x_{12}, \tilde{y}) + \left(-\frac{\partial S_2(x_{12}, \tilde{y})}{\partial y_0} \right) S_2(x_{02}, \tilde{y}) \\ - \left(-\frac{\partial S_2(x_{01}, \tilde{y})}{\partial y_0} \right) \Bigg] \end{aligned} \tag{3.22}$$

By the chain rule, we obtain for the initial condition of $\frac{\partial S_2}{\partial y_0}$:

$$\begin{aligned} -\frac{\partial S_2}{\partial y_0}_{|\tilde{y}=0}(x_{01}, \tilde{y}) &= \frac{\partial S_2}{\partial \tilde{y}}_{|\tilde{y}=0}(x_{01}, \tilde{y}) - \frac{\partial S_2}{\partial y_0}(x_{01}, 0) \\ &= \bar{\alpha} \int \frac{d^2 x_2}{2\pi} \frac{x_{01}^2}{x_{02}^2 x_{12}^2} \left[S^2(x_{02}, y_0) S^2(x_{12}, y_0) - S^2(x_{01}, y_0)\right] - 2S(x_{01}, y_0) \frac{\partial}{\partial y_0} S(x_{01}, y_0) \\ &= \bar{\alpha} \int \frac{d^2 x_2}{2\pi} \frac{x_{01}^2}{x_{02}^2 x_{12}^2} \left[S(x_{02}, y_0) S(x_{12}, y_0) - S(x_{01}, y_0)\right]^2 \end{aligned} \tag{3.23}$$

where in the second line, we employed the condition Eq.(3.21). Interestingly one can see that, Eq.(3.21) is exactly in the same form as Eq.(3.14) in which $\mathcal{G}$ is replaced by $(-\partial S_2/\partial y_0)$ and $\mathcal{U}$ is replaced by S_2. In other words, the diffraction problem and the ancestry problem are governed by the same type of equation. However, we still cannot relate different initial conditions for those two problems. In the next section, numerical calculations will be implemented to see the relation between their solutions.

3.3 Numerical calculations

3.3.1 Diffraction from the Kovchegov - Levin equation

The strategy is to solve numerically a set of two BK equations Eq.(3.20) and Eq.(2.20) for S_2 and S, respectively, where the result of the latter is used as the initial condition (up to a square) of the former. Instead of $S(x_{01}, Y)$, the amplitude $N(x_{01}, Y) = 1 - S(x_{01}, Y)$, which obeys the BK equation Eq.(2.21), is now employed. Performing the following (modified) Fourier transform:

$$\tilde{N}(k, Y) = \int \frac{d^2x_{01}}{2\pi x_{01}^2} e^{ik\cdot x_{01}} N(x_{01}, Y) \tag{3.24}$$

with the conjugate transverse momentum k, one can get:

$$\partial_Y \tilde{N}(k, Y) = \bar{\alpha}\chi\left(-\partial_{\ln|k|^2}\right)\tilde{N}(k, Y) - \bar{\alpha}\left[\tilde{N}(k, Y)\right]^2 \tag{3.25}$$

where $\chi(\gamma)$ is the eigenfunction of the BFKL kernel given by Eq.(1.33). This equation is implemented and solved numerically using a code developed by S. Munier for fixed impact parameter.

We start with the MV initial condition Eq.(2.22) in which the parameters are chosen to be $Q_{MV} = 1\,\text{GeV}$ and $\Lambda_{\text{QCD}} = 200\,\text{MeV}$ and transform it to the momentum space. $\tilde{N}_{MV}(k, 0)$ is then evolved to the rapidity y_0 to get $\tilde{N}(k, y_0)$, which is, in turn, transformed back to the transverse position space. We calculated the quantity $2N(x_{01}, y_0) - N^2(x_{01}, y_0)$, which is served as the initial condition for the Kovchegov - Levin equation. The Fourier transform of $N(x_{01}, Y)$ is then evolved further for $\tilde{y}_0 = Y - y_0$ units of rapidity. This procedure is repeated for different values of y_0 between 0 and Y. The numerical y_0 - derivative is performed in the transverse position space to get the rapidity gap distribution $d\sigma_{\text{diff}}/dy_0$, which is normalized by the total cross section $\sigma_{\text{tot}} = 2N(x_{01}, Y)$. The result is plotted as a function of y_0 for chosen values of x_{01}. The distribution is then fitted to the function of the form:

$$\frac{1}{\sigma_{\text{tot}}}\frac{d\sigma_{\text{diff}}}{dy_0} = c \times \left[\frac{\bar{\alpha}Y}{\bar{\alpha}y_0\bar{\alpha}(Y - y_0)}\right]^{3/2} \exp\left\{-\frac{\ln^2\left[x_{01}^2 Q_s^2(Y)\right]}{2\bar{\alpha}(Y - y_0)\chi''(\gamma_0)}\right\} \tag{3.26}$$

where c is an overall constant, and $Q_s(Y)$ is determined from the numerical data with the condition $N(x_{01} = 2/Q_s(Y), Y) = 1/2$.

For $\bar{\alpha}Y = 20$, the data is taken from [35] and shown in Fig. 3.4. The asymptotic formula Eq.(3.26) describes noticeably well the numerical data. For values of x_{01} deep inside the scaling region, the curve is quite symmetric and one can approximate it by the formula Eq.(3.10). The effect of the exponential (Gaussian) term becomes important when the dipole size is around the transition to non-scaling region, which leads to a significant suppression.

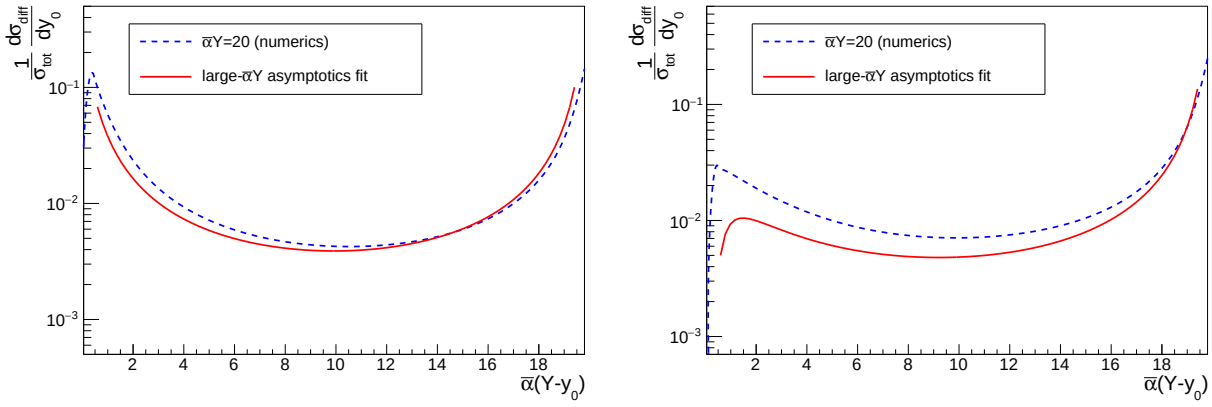

(A) $x_{01} = 10^{-20}$ (B) $x_{01} = 10^{-22}$

FIGURE 3.4: Rapidity gap distribution for $\bar{\alpha}Y = 20$ for different values of x_{01}. The red continuous line is the asymptotic form Eq.(3.26)

3.3.2 Ancestry problem

For the ancestry problem, we deal with a set of two equations Eq.(3.14) and Eq.(3.11) for $\mathcal{G}$ and $\mathcal{U}$, respectively. In the same manner as above, one introduces $\mathcal{W}(r, Y) = 1 - \mathcal{U}(r, Y)$, which satisfies the BK equation of the type Eq.(2.21). The Fourier transform of the Eq.(3.14) in term of $\mathcal{W}$ reads:

$$\partial_Y \tilde{\mathcal{G}}(k, Y, y_0) = \bar{\alpha}\chi\left(-\partial_{\ln|k|^2}\right)\tilde{\mathcal{G}}(k, Y, y_0) - 2\bar{\alpha}\tilde{\mathcal{W}}(k, Y)\tilde{\mathcal{G}}(k, Y, y_0) \tag{3.27}$$

with the initial condition: $\tilde{\mathcal{G}}(k, Y = y_0, y_0) = \bar{\alpha}\mathcal{W}^2(k, y_0)$. The equation Eq.(3.26) differs from Eq.(3.24) just in the second term in the right hand side, thus one can modify the code solving the BK equation in the momentum space mentioned above to solve this type of equation.
We also notice that, the initial condition for $\mathcal{U}$ (or $\mathcal{W}$), which is the Heaviside function given by Eq.(3.12), is hard to be implemented numerically since its Fourier transform is oscillated. However, one can observe that for small x_{01}, $1 - S_{MV}(x_{01}) \sim x_{01}^2 Q_{MV}^2 = e^{\ln x_{01}^2 Q_{MV}^2}$. Thus, the MV initial condition is steeper than $e^{\gamma_0 \ln x_{01}^2 Q_{MV}^2}$, with $\gamma_0 \simeq 0.627549$. Therefore, according to the discussion on the solution of the BK equation in the previous chapter, one can replace the Heaviside step function by the MV amplitude for the initial condition for $\mathcal{W}$.

The numerical implementation of the ancestry problem is thus straightforward. First we employ the BK code above to evolve $\mathcal{W}$ to y_0 between 0 and Y from the MV amplitude. Using $\bar{\alpha}\tilde{\mathcal{W}}^2(k, y_0)$ (from Eq.(3.15)) as the initial condition for $\mathcal{G}$ and the modified version of the BK code for solving Eq.(3.27), $\mathcal{G}$ is then evolved from y_0 to Y. This procedure is repeated for many different values of y_0. The result is then normalized by N, which is asymptotically identical to the probability P to have at least one dipole crossing the saturation scale of the nucleus in the previous discussion, and plotted as a function of $Y - y_0$. In Fig. 3.5, the numerical solutions are plotted for different values of x_{01} and fitted to the function of the form Eq.(3.27). The numerical calculations for the diffraction problem with the same values of x_{01} are also superimposed. We see that, the behavior of the solutions of two problems are the same, which is fairly symmetric deep inside the scaling region and suppressed by a Gaussian term when going beyond. In addition, when going deep into the scaling region by choosing the value of x_{01} such that the curves are symmetric, the rapidity gap distribution and the distribution of the most recent common agree (see Fig. 3.6). Thus the numerical calculations show that the solutions of the diffraction and the ancestry problems

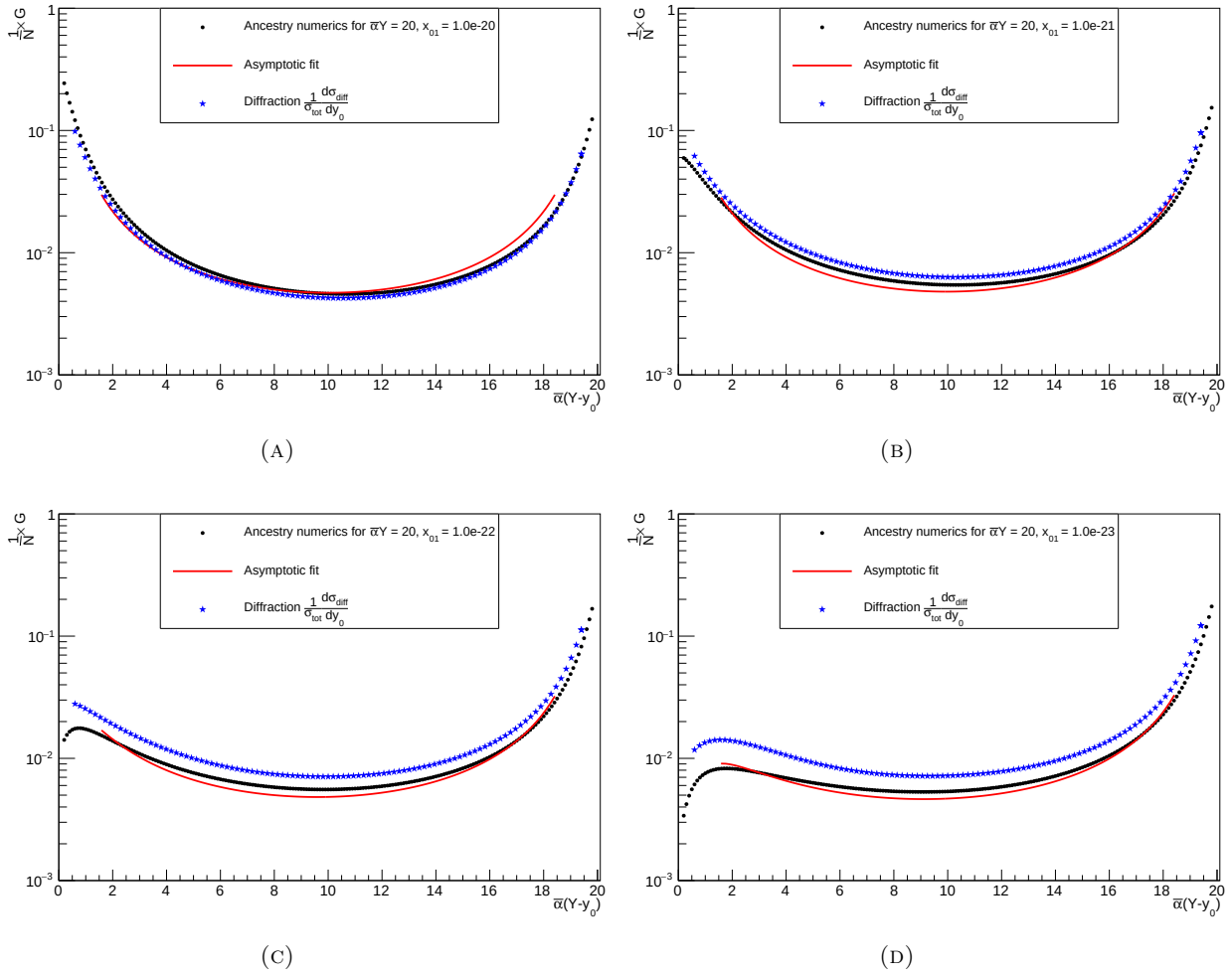

(A) (B)

(C) (D)

FIGURE 3.5: Normalized distribution $\mathcal{G}$ for $\bar{\alpha}Y = 20$ at different values of x_{01}. Rapidity gap distribution is also superimposed to compare.

asymptotically coincide. Another interesting point is that, when plotting the distribution Eq.(3.16) in which γ_0 is replaced by $\bar{\gamma} = 1$, there is a good agreement between the BRW prediction and the numerical data (see Fig. 3.6). This is the reproduction of the result shown in [38].

When evolving the solution of the ancestry equation to a higher value of rapidity, say $\bar{\alpha}Y = 40$, it gets closer to the distribution Eq.(3.16) predicted from the genealogy of branching random walks (see Fig.3.7). Furthermore, in the region $\bar{\alpha}(Y - y_0) \sim \bar{\alpha}Y$, which is corresponding to the high-mass region in the diffraction problem, the solution approaches the BRW prediction when x_{01} decreases. Those observations may suggest that the asymptotic solution of the ancestry problem (and hence of the diffraction problem) could be bounded from above by the BRW-predicted distribution. This, however, needs to have further numerical tests.

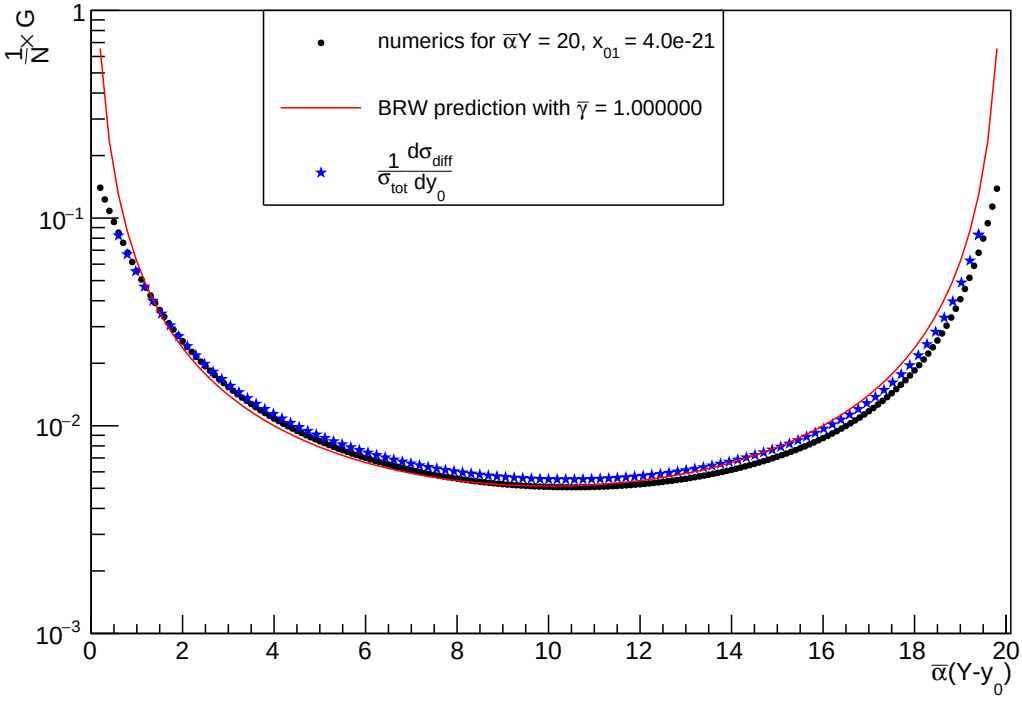

FIGURE 3.6: The asymptotic behavior of the solutions of different processes deep inside the scaling region. The black curve is the distribution of the most recent common ancestor, while the blue curve is the rapidity gap distribution in the diffractive onium-nucleus scattering. The red curve takes the form of the BRW prediction in which $1/\gamma_0$ is replaced by $1/\bar{\gamma}$ with $\bar{\gamma} = 1$.

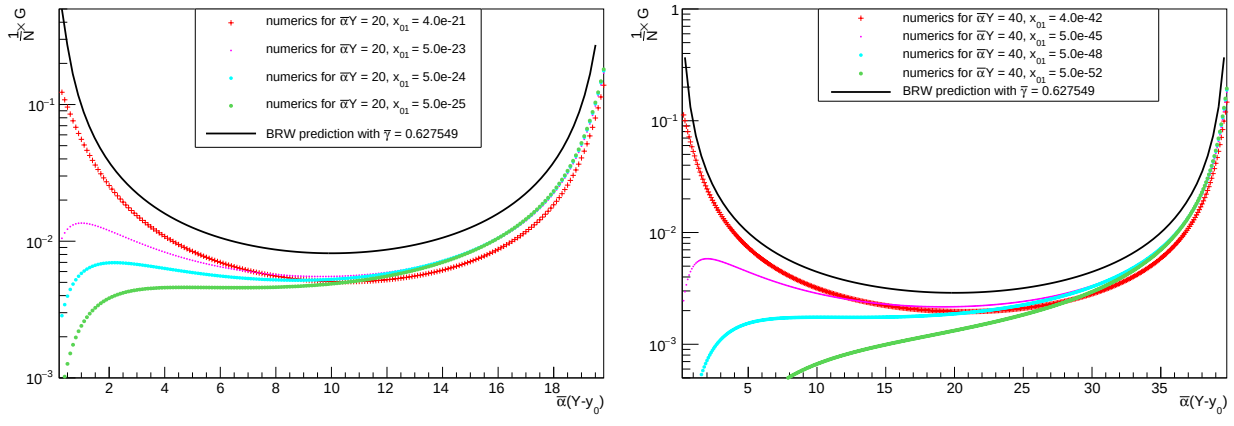

(A) (B)

FIGURE 3.7: The behavior of the solution to the ancestry problem for different values of x_{01} with: (A) $\bar{\alpha}Y = 20$ and (B) $\bar{\alpha}Y = 40$.

Conclusion

In the report, we reviewed some aspects of small-x physics and the color dipole formulation of the quantum chromodynamics on the light-cone. Partonic evolutions at high energy in the dipole framework were also introduced for its use in later discussions on the diffraction.

The main results of the report came from the discussions on the diffraction in the high-energy onium - nucleus scattering and the ancestry problem of the onium evolution. Using a similar argument as in the derivation of the BFKL and BK equations, an equation for the ancestry problem was derived containing an ingredient which evolves according to the BK equation. The ancestry equation was then shown to be same as the equation for the rapidity gap distribution which was deduced from the Kovchegov - Levin equation but with different initial conditions. Numerical results showed that the asymptotic solutions of those two equations truly coincide. Also, an analogy to the genealogy of one-dimensional branching random walks (BRW) addressed by Derrida and Mottishaw was given. This analogy was then tested numerically yielding a good agreement between the numerical data and the BRW prediction deep inside the scaling region with an ad hoc normalization factor.

The discussions in the report suggest several works to do beyond. The global constant in Eq.(3.10) is unknown, which requires further analytical and numerical determinations of its value. In fact, we believe that we now have a derivation of the constant which we are presently checking and will aim at publishing it. In addition, the calculation of sub-asymptotic corrections is an interesting consideration to understand the behavior of the evolution at moderate rapidities. Also, the good numerical agreement between the ancestry and the diffraction problems puts forward a challenging question: why the Kovchegov - Levin and the ancestry equations mathematically converge to the same solution in the asymptotic region?

Appendix A

QCD LCPT rules

1. Draw all diagrams for a given process at the desired order in the coupling constant, including all possible orderings of the interaction vertices in the light-cone time x^+. Assign a four-momentum k^μ to each line such that it is on mass shell. Each vertex conserves only the k^+ and $k_\perp$ components of the four-momentum.

2. With quarks associate spinors u_σ(k) or $v_\sigma(k)$ which is normalized as:

$$\bar{u}_\sigma(k)\gamma_\mu u_\rho(k) = \bar{v}_\sigma(k)\gamma_\mu v_\rho(k) = 2k_\mu\delta_{\sigma\rho} \tag{A.1}$$

3. With a gluon associate a polarization vector $\epsilon^\mu_\lambda(k)$ which satisfies $\epsilon^+_\lambda = 0$, $\epsilon_\lambda(k)\cdot k = 0$ and $\epsilon^2(k) = 1$.

4. For each internal line, include a factor: $\frac{\theta(k^+)}{k^+}$

5. For each intermediate state, there is a factor:

$$\frac{1}{\sum_{\text{init}} k^- - \sum_{\text{interm}} k^- + i\epsilon} \tag{A.2}$$

   where thsums are over all particles in the initial and intermediate states respectively.

6. For vertices include following factors:

   (a) Quark-gluon vertex

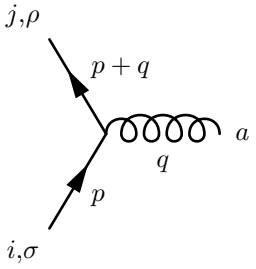

$$-g_s\bar{u}_{\rho j}(p+q)\not{\epsilon}_\lambda(q)(t^a)_{ji}u_{\sigma i}(p) \tag{A.3}$$

(b) Three-gluon vertex (all momenta flow into the vertex)

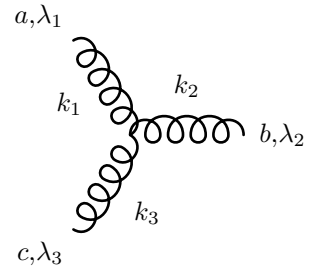

$$
\begin{aligned}
-ig_s f^{abc}\big[&(k_1-k_3)\cdot\epsilon^*_{\lambda_2}(k_2)\epsilon_{\lambda_1}(k_1)\cdot\epsilon_{\lambda_3}(k_3)\\
&+(k_3-k_2)\cdot\epsilon_{\lambda_1}(k_1)\epsilon_{\lambda_3}(k_3)\cdot\epsilon^*_{\lambda_2}(k_2)\\
&+(k_2-k_1)\cdot\epsilon_{\lambda_3}(k_3)\epsilon_{\lambda_1}(k_1)\cdot\epsilon^*_{\lambda_2}(k_2)\big]
\end{aligned}
\tag{A.4}
$$

(c) Four-gluon vertex

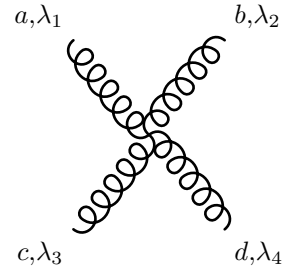

$$
\begin{aligned}
g^2\big[&f^{abe}f^{cde}(\epsilon_{\lambda_1}\cdot\epsilon_{\lambda_3}\epsilon^*_{\lambda_2}\cdot\epsilon^*_{\lambda_4}-\epsilon_{\lambda_1}\cdot\epsilon^*_{\lambda_4}\epsilon_{\lambda_3}\cdot\epsilon^*_{\lambda_2})\\
&+f^{ace}f^{bde}(\epsilon_{\lambda_1}\cdot\epsilon^*_{\lambda_2}\epsilon_{\lambda_3}\cdot\epsilon^*_{\lambda_4}-\epsilon_{\lambda_1}\cdot\epsilon^*_{\lambda_4}\epsilon_{\lambda_3}\cdot\epsilon^*_{\lambda_2})\\
&+f^{ade}f^{bce}(\epsilon_{\lambda_1}\cdot\epsilon^*_{\lambda_2}\epsilon_{\lambda_3}\cdot\epsilon^*_{\lambda_4}-\epsilon_{\lambda_1}\cdot\epsilon_{\lambda_3}\epsilon^*_{\lambda_2}\cdot\epsilon^*_{\lambda_4})\big]
\end{aligned}
\tag{A.5}
$$

7. For instantaneous terms, include following factors:

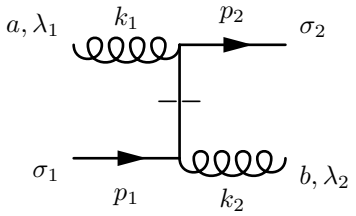

$$
\begin{aligned}
&g_s^2\bar{u}_{\sigma_2 j}(p_2)\not{\epsilon}_{\lambda_1}(k_1)\frac{\gamma^+}{2(p_1^+-k_2^+)}\not{\epsilon}^*_{\lambda_2}(k_2)\\
&\quad\times(t^a t^b)_{ij}u_{\sigma_1 i}(p_1)
\end{aligned}
\tag{A.6}
$$

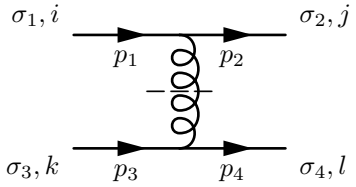

$$
\begin{aligned}
&g_s^2\bar{u}_{\sigma_2 j}(p_2)\gamma^+(t^a)_{ij}u_{\sigma_1 i}(p_1)\frac{1}{(p_1^+-p_1^+)^2}\\
&\quad\times\bar{u}_{\sigma_4 l}(p_4)\gamma^+(t^a)_{lk}u_{\sigma_3 k}(p_3)
\end{aligned}
\tag{A.7}
$$

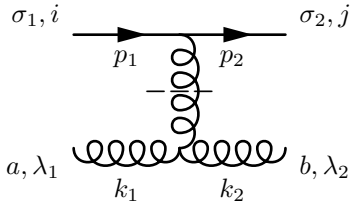

$$
\begin{aligned}
&-g_s^2\bar{u}_{\sigma_2 j}(p_2)\gamma^+(t^c)_{ji}u_{\sigma_1 i}(p_1)\\
&\quad\times\frac{k_1^+ + k_2^+}{(k_1^+-k_2^+)^2}if^{abc}\epsilon^*_{\lambda_2}\cdot\epsilon_{\lambda_1}
\end{aligned}
\tag{A.8}
$$

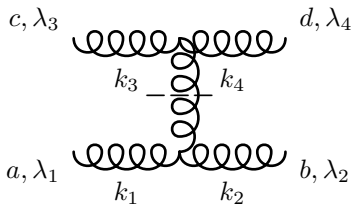

$$
\begin{aligned}
&g_s^2 f^{abe}f^{cde}\epsilon^*_{\lambda_2}\epsilon_{\lambda_1}\epsilon^*_{\lambda_4}\epsilon_{\lambda_3}\\
&\quad\times\frac{(k_1^+ + k_2^+)(k_4^+ + k_3^+)}{(k_1^+-k_2^+)^2}
\end{aligned}
\tag{A.9}
$$

8. For each independent momentum k^μ integrate with the measure:

$$\int \frac{dk^+ d^2k_\perp}{2(2\pi)^3} \tag{A.10}$$

and sum over internal helicities and colors.

9. There is a factor (-1) for each fermion loop and for each fermion line beginning and ending at the initial state, and usual symmetric factors.

Appendix B

Derivation of the onium light-cone wave function with one soft gluon

Here we will derive the onium light-cone wave function containing one soft gluon in momentum space, namely the formula Eq.(2.5). Notations used in this appendix is same as in Chapter 2.

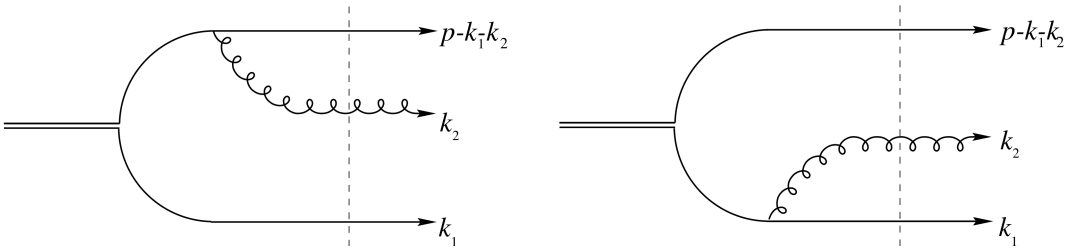

(A) (B)

FIGURE B.1: Onium wave function with one soft gluon. The dashed lines denote the intermediate state (Lower line is quark and the upper one is anti-quark)

The onium wave function with one soft gluon $\psi^{(1)a}_{\alpha\beta}(k_{1\perp}, k_{2\perp}; z_1, z_2)$ evaluated at some intermediate point (as indicated in the Fig.B.1) is given by the product of the bare wave function and the amplitude of one gluon emission. Since there are two contributions corresponding to the gluon being emitted from quark or anti-quark, one has:

$$\psi^{(1)a}_{\alpha\beta}(k_{1\perp}, k_{2\perp}; z_1, z_2) = \sum_{\sigma} \left(\psi^{(0)}_{\alpha\beta}(k_{1\perp}, z_1)(-\mathcal{M}_{\beta\sigma}(k_{2\perp})) + \psi^{(0)}_{\alpha\beta}(k_{1\perp} + k_{2\perp}, z_2)\mathcal{M}_{\sigma\alpha}(k_{2\perp}) \right) \tag{B.1}$$

where $\psi^{(0)}$ is the bare onium wave function, $\mathcal{M}(k_{2\perp})$ is the amplitude of the gluon emission, α and β are spinor indices of the original quark and anti-quark, respectively, and σ is the spinor index of the produced quark or anti-quark (together with the gluon). The sum is taken over all polarizations of the produced quark or anti-quark.

The first term corresponds to Fig.B.1A with gluon being emitted from anti-quark, while the second term is represented by Fig.B.1B. Apply the QCD LCPT rules for the first term, we have (neglecting for a while

the minus sign):

$$\psi^{(0)}_{\alpha\beta}(k_{1\perp},z_1)\mathcal{M}_{\beta\sigma}(k_{2\perp}) = \psi^{(0)}_{\alpha\beta}(k_{1\perp},z_1)(-g_s t^a)\frac{\bar{v}_\beta(p-k_1)\not{\epsilon}^{\lambda}_2(k_2)v_\sigma(p-k_1-k_2)\theta((p-k_1)^+)}{(p-k_1)^+} \times \frac{1}{k_2^- + k_1^- + (p-k_2-k_1)^- - p^-} \tag{B.2}$$

Since $z_2 \ll z_1, 1-z_1$, k_2^- will dominate the denominator in the second line of Eq.(B.2). So:

$$\frac{1}{k_2^- + k_1^- + (p-k_2-k_1)^- - p^-} \simeq \frac{1}{k^-} \tag{B.3}$$

We also have:

$$\bar{v}_\beta(p-k_1)\not{\epsilon}^{\lambda}_2(k_2)v_\sigma(p-k_1-k_2) \simeq 2\delta_{\beta\sigma}\sqrt{(p-k_1)^+(p-k_1-k_2)^+}\epsilon_2^{\lambda-} \simeq 2\delta_{\beta\sigma}(p-k_1)^+\epsilon_2^{\lambda-} \tag{B.4}$$

Hence:

$$\psi^{(0)}_{\alpha\beta}(k_{1\perp},z_1)\mathcal{M}_{\beta\sigma}(k_{2\perp}) \simeq \psi^{(0)}_{\alpha\beta}(k_{1\perp},z_1)(-g_s t^a)\frac{2\delta_{\beta\sigma}\epsilon_2^{\lambda-}\theta((p-k_1)^+)}{k^-} \tag{B.5}$$

With the same spirit, the second term in Eq.(B.1) reads:

$$\psi^{(0)}_{\alpha\beta}(k_{1\perp}+k_{2\perp},z_2)\mathcal{M}_{\sigma\alpha}(k_{2\perp}) \simeq \psi^{(0)}_{\alpha\beta}(k_{1\perp}+k_{2\perp},z_2)(-g_s t^a)\frac{2\delta_{\sigma\alpha}\epsilon_2^{\lambda-}\theta(k_1^+)}{k^-} \tag{B.6}$$

Substituting Eq.(B.5) and Eq.(B.6) into Eq.(B.1), one finally obtains:

$$\psi^{(1)a}_{\alpha\beta}(k_{1\perp},k_{2\perp};z_1,z_2) = 2g_s t^a\left[\psi^{(0)}_{\alpha\beta}(k_{1\perp},z_1) - \psi^{(0)}_{\alpha\beta}(k_{1\perp}+k_{2\perp},z_2)\right]\frac{k_{2\perp}\cdot\epsilon^{\lambda}_{2\perp}}{k^2_{2\perp}} \tag{B.7}$$

where we have used the fact that $k^- = k^2_{2\perp}/k^+$, $\epsilon^- = (k_{2\perp}\cdot\epsilon^{\lambda}_{2\perp})/k^+$ and $0 < z_1 < 1$.

Bibliography

[1] E. Kuraev, V. Lipatov, and V. Fadin. "The pomeranchuk singularity in non-abelian gauge theories". In: *Sov. Phys. JETP.* 45 (1977), p. 199.

[2] Y. Balisky and L.N. Lipatov. "The pomeranchuk singularity in quantum chromodynamics". In: *Sov. J. Nucl. Phys.* 28 (1978), p. 822.

[3] L.N. Lipatov. In: *Sov. Phys. JETP* 63 (1986), p. 904.

[4] I. Balitsky. "Operator expansion for high-energy scattering". In: *Nucl. Phys. B* 463.1 (1996), p. 99.

[5] Yuri V. Kovchegov. "Unitarization of the BFKL Pomeron on a nucleus". In: *Phys. Rev. D* 61.7 (2000), p. 074018.

[6] A.H. Mueller. "Soft gluons in the infinite-momentum wave function and the BFKL pomeron". In: *Nucl. Phys. B* 415.2 (1994), p. 373.

[7] A.H. Mueller and Bimal Patel. "Single and double BFKL pomeron exchange and a dipole picture of high energy hard processes". In: *Nucl. Phys. B* 425.3 (1994), p. 471.

[8] A.H. Mueller. "Unitarity and the BFKL pomeron". In: *Nucl. Phys. B* 437.1 (1995), p. 107.

[9] D. J. Gross and F. Wilczek. "Ultraviolet behavior of non-abelian gauge theories". In: *Phys. Rev. Lett.* 30.26 (1973), p. 1343.

[10] H. Fritzsch, M. Gell-Mann, and H. Leutwyler. "Advantages of the color octet gluon picture". In: *Phys. Lett. B* 47.4 (1973), p. 365.

[11] S. Weinberg. "General theory of broken local symmetries". In: *Phys. Rev. D* 7.4 (1973), p. 1068.

[12] M. E. Peskin and D. V. Schroeder. *An introduction to quantum field theory.* Addison-Wesley Publishing Company, 1995.

[13] Y. V. Kovchegov and E. Levin. *Quantum Chromodynamics at High Energy.* Cambridge University Press, 2012.

[14] P. A. M . Dirac. "Forms of relativistic dynamics". In: *Rev. Mod. Phys.* 21.3 (1949), p. 392.

[15] S. Weinberg. "Dynamics at infinite momentum". In: *Phys. Rev.* 150.4 (1966), p. 1313.

[16] L. Susskind. "Model of Self-Induced Strong Interactions". In: *Phys. Rev.* 165.5 (1968), p. 1535.

[17] G. P. Lepage and S. J. Brodsky. "Exclusive processes in perturbative quantum chromodynamics". In: *Phys. Rev. D* 22.9 (1980), p. 2157.

[18] S. J. Brodsky and G. P Lepage. "Exclusive processes in quantum chromodynamics". In: *Perturbative QCD.* Ed. by A. H. Mueller. World Scientific Publishing Co, 1989, pp. 93–240. DOI: 10.1142/9789814503266_0002.

[19] S. J. Brodsky, H. C. Pauli, and S. S. Pinsky. "Quantum chromodynamics and other field theories on the light cone". In: *Phys. Rep.* 301 (1998), p. 299.

[20] C. G. Callan and David J. Gross. "High-Energy Electroproduction and the Constitution of the Electric Current". In: *Phys. Rev. Lett.* 22.4 (1969), p. 156.

[21] J. D. Bjorken and E. A. Paschos. "Inelastic Electron-Proton and γ-Proton Scattering and the Structure of the Nucleon". In: *Phys. Rev.* 185.5 (1969), p. 1975.

[22] V. N. Gribov and L. N. Lipatov. "Deep inelastic e p scattering in perturbation theory". In: *Sov. J. Nucl. Phys.* 15 (1972). [Yad. Fiz.15,781(1972)], p. 438.

[23] Yuri L. Dokshitzer. "Calculation of the Structure Functions for Deep Inelastic Scattering and e+ e- Annihilation by Perturbation Theory in Quantum Chromodynamics." In: *Sov. Phys. JETP* 46 (1977). [Zh. Eksp. Teor. Fiz.73,1216(1977)], p. 641.

[24] G. Altarelli and G. Parisi. "Asymptotic freedom in parton language". In: *Nucl. Phys. B* 126.2 (1977), p. 298.

[25] ZEUS Collaboration; M. Derrick et. al. "Measurement of the Proton Structure Function F2 in ep Scattering at HERA". In: *Phys. Lett. B* 316.2-3 (1993), p. 412.

[26] ZEUS Collaboration; M. Derrick et. al. "Measurement of the proton structure function F2 from the 1993 HERA data". In: *Z. Phys. C* 65.3 (1995), p. 379.

[27] L.V. Gribov, E.M. Levin, and M.G. Ryskin. "Semihard processes in QCD". In: *Physics Reports* 100.1 (1983), p. 150.

[28] A.H. Mueller and Jianwei Qiu. "Gluon recombination and shadowing at small values of x". In: *Nucl. Phys. B* 268.2 (1986), p. 427.

[29] J. R. Forshaw and D. A. Ross. *Quantum Chromodynamics and the Pomeron*. Cambridge Lecture Notes in Physics. Cambridge University Press, 1997. DOI: 10.1017/CBO9780511524387.

[30] Z. Chen and A.H. Mueller. "The dipole picture of high energy scattering, the BFKL equation and many gluon compound states". In: *Nucl. Phys. B* 451.3 (1995), p. 579.

[31] G.'t Hooft. "A planar diagram theory for strong interactions". In: *Nucl. Phys. B* 72.3 (1974), p. 461.

[32] G. P. Salam. "Quarkonium Scattering at High Energies". PhD Dissertation. University of Cambridge, 1996.

[33] S. Munier. "Statistical physics in QCD evolution towards high energies". In: *Sci. China Phys. Mech. Astron.* 58.8 (2015), p. 81001.

[34] A.H Mueller and D.N Triantafyllopoulos. "The energy dependence of the saturation momentum". In: *Nucl. Phys. B* 640.1 (2002), p. 331.

[35] A. H. Mueller and S. Munier. "Rapidity gap distribution in diffractive deep-inelastic scattering and parton genealogy". In: *Report CPHT-RR033.052018* (2018). arXiv: 1805.02847 [hep-ph].

[36] A.H. Mueller and S. Munier. "On parton number fluctuations at various stages of the rapidity evolution". In: *Phys. Lett. B* 737 (2014), p. 303.

[37] A. H. Mueller and S. Munier. "Phenomenological picture of fluctuations in branching random walks". In: *Phys. Rev. E* 90.4 (2014), p. 042143.

[38] A. H. Mueller and S. Munier. "Diffractive electron-nucleus scattering and ancestry in branching random walks". In: *Report CPHT-RR035.052018* (2018). arXiv: 1805.09417 [hep-ph].

[39] B. Derrida and P. Mottishaw. "On the genealogy of branching random walks and of directed polymers". In: *EPL (Europhysics Letters)* 115.4 (2016), p. 40005.

[40] M. L. Good and W. D. Walker. "Diffraction Dissociation of Beam Particles". In: *Phys. Rev.* 120.5 (1960), p. 1857.

[41] Yuri V. Kovchegov and Eugene Levin. "Diffractive dissociation including multiple pomeron exchanges in high parton density QCD". In: *Nucl. Phys. B* 577.1 (2000), p. 221.